https://doi.org/10.5194/egusphere-2023-2018
Preprint. Discussion started: 20 September 2023

Wintertime Extreme Warming Events in the High Arctic: Characteristics, Drivers, Trends, and the Role of Atmospheric Rivers

Weiming Ma[1], Hailong Wang[1], Gang Chen[2], Yun Qian[1], Ian Baxter[3,4], Yiling Huo[1], Mark W. Seefeldt[5]

[1]Atmospheric Sciences and Global Change Division, Pacific Northwest National Laboratory, Richland, WA, USA
[2]Department of Atmospheric and Oceanic Sciences, University of California Los Angeles, Los Angeles, CA, USA
[3]Department of Geography, University of California, Santa Barbara, Santa Barbara, CA, USA
[4]Earth Research Institute, University of California, Santa Barbara, Santa Barbara, CA, USA
[5]National Snow Ice and Data Center, University of Colorado Boulder, Boulder, CO, USA

Correspondence to: Weiming Ma (weiming.ma@pnnl.gov), Hailong Wang (Hailong.Wang@pnnl.gov)

Abstract. An extreme warming event near the North Pole, with temperature rising above 0℃, was observed in late December 2015. This specific event has been attributed to cyclones and their associated moisture intrusions. However, little is known about the characteristics and drivers of similar events in the historical record. Here, using data from ERA5, we study these winter extreme warming events with temperature above 0℃ over the high Arctic (poleward of 80°N) occurred during 1980-2021. In ERA5, such extreme events can only be found over the Atlantic sector. They occur rarely, with a seasonal occurrence frequency less than one over most of the regions. Furthermore, even when occurring, they tend to be short-lived, with the majority of the events lasting for less than a day. By examining their surface energy budget, we found that these events transition with increasing latitude from a regime dominated by turbulent heat flux into the one dominated by downward longwave radiation. Blockings over the northern Eurasia are identified as a key ingredient in driving these events, as they can effectively deflect the eastward propagating cyclones poleward, leading to intense moisture and heat intrusions into the high Arctic. Using an atmospheric river (AR) detection algorithm, the roles of ARs in driving these events are explicitly quantified. The importance of ARs in inducing these events increases with latitude. Poleward of about 83°N, ARs are the direct driver for 100% of these events, corroborating the indispensable roles ARs played in driving these events. Over the past four decades, both the frequency, duration, and magnitude of these events have been increasing significantly. As the Arctic continues to warm, these events are likely to increase in both frequency, duration and magnitude, with great implications for the local sea ice, hydrological cycle and ecosystem.

1 Introduction

In recent decades, the Arctic has experienced dramatic changes, with its surface warming at a rate substantially faster than the rest of the world (Previdi et al., 2021; Rantanen et al., 2022; Serreze and Barry, 2011). Such amplified Arctic warming is especially pronounced in winter (Zhang et al., 2021b). Several key mechanisms have been proposed to explain the amplified warming in the Arctic. These proposed mechanisms include local feedbacks, such as the ice-albedo feedback (Screen and

https://doi.org/10.5194/egusphere-2023-2018
Preprint. Discussion started: 20 September 2023

Simmonds, 2010; Dai et al., 2019; Kumar et al., 2010), water vapor and cloud feedback (Beer and Eisenman, 2022; Vavrus, 2004), and lapse rate feedback (Stuecker et al., 2018; Pithan and Mauritsen, 2014), and non-local mechanisms that consist of both ocean and atmospheric heat transport (Singh et al., 2017; Graversen and Langen, 2019; Hwang et al., 2011; Graversen and Burtu, 2016). The atmospheric component can be further decomposed into a sensible heat and a latent heat (moisture) component, with the latent heat component playing a more important role (Graversen and Burtu, 2016). Concurrent with this warming trend is the rapid reduction in both sea ice extent and thickness (Serreze and Stroeve, 2015; Stroeve and Notz, 2018). Although it is still highly debated, Arctic warming and sea ice loss can reduce the meridional temperature gradient and have thus been hypothesized to modulate extreme weather events over mid-latitudes through their influence on large-scale circulation there (Screen et al., 2018; Cohen et al., 2014; Zou et al., 2021; Ma et al., 2021). In addition to these strong trends in the mean climate, the Arctic warming may also lead to more frequent occurrence of local synoptic weather extremes, ranging from rapid sea ice loss (Wang et al., 2020; Gimeno et al., 2019; Park et al., 2015; Zhang et al., 2023), rain-on-snow events (Serreze et al., 2021; Dou et al., 2021), extreme Arctic cyclones (Parker et al., 2022; Rinke et al., 2017; Crawford et al., 2022) and heatwaves (Woods and Caballero, 2016; Graham et al., 2017; Dobricic et al., 2020). The increases and intensification of these weather extremes are expected to exert profound impacts on the Arctic ecosystem and local communities (Amstrup et al., 2010; Post et al., 2013; Ford et al., 2021).

It has been found that, besides contributing to the mean warming over the Arctic, atmospheric moisture transport can exert an important influence on many aspects of the Arctic climate. For example, enhanced atmospheric moisture transport into the Arctic in spring can lead to anomalous downward longwave radiation and thus precondition the sea ice for a more rapid melt in the subsequent months (Schröder et al., 2014; Kapsch et al., 2013; Mortin et al., 2016). Spring atmospheric moisture convergence can thus serve as an important predictor for summer minimum sea ice extent. In addition to its effects on the sea ice, recent increases in the Arctic river discharges have also been found to be primarily driven by an increase in poleward atmospheric moisture transport (Zhang et al., 2013). As sea ice continues to decline and atmospheric moisture transport continues to increase, the interannual variability of Arctic precipitation is expected to be increasingly controlled by atmospheric moisture transport (Bintanja et al., 2020).

Studies have shown that the bulk of atmospheric moisture transported into the Arctic is accomplished by episodes of extreme moisture transport events, termed Arctic moisture intrusions or atmospheric rivers (ARs) (Zhang et al., 2023; Nash et al., 2018). ARs, filaments of intense moisture transport in the atmosphere, have traditionally been identified as mid-latitude phenomenon. Early studies found that, despite occupying only about 10% of the mid-latitude circumference, ARs are responsible for more than 90% of the poleward moisture transport there (Zhu and Newell, 1998). ARs have been studied extensively for mid-latitude regions due to their important contribution to the regional hydrological cycle (Waliser and Guan, 2017; Lamjiri et al., 2017; Leung and Qian, 2009; Pan and Lu, 2020; Viale et al., 2018; Lavers and Villarini, 2015). In recent years, it gets increasingly recognized that ARs also exert considerable impacts on the Arctic climate (Nash et al., 2018; Zhang et al., 2023; Hegyi and Taylor, 2018). When a large amount of moisture carried by ARs intrudes into the Arctic in a short period of time, the rapid moistening of the lower atmosphere and the resulting cloudy condition and enhanced downward

https://doi.org/10.5194/egusphere-2023-2018
Preprint. Discussion started: 20 September 2023

longwave radiation can lead to a rapid rise in surface temperature and substantial sea ice loss. Therefore, ARs are potentially an important driver of extreme events over the Arctic region.

In late December 2015, the high Arctic near the pole experienced an episode of extreme warming event, with surface temperature exceeding 0℃ (Graham et al., 2017; Binder et al., 2017; Moore, 2016). Subsequent examination reveals the short-lived nature of this event, with the duration of staying above 0℃ for less than an hour. This event is driven by an AR-like moisture plume carried into the high Arctic by a cyclone. While this event has been studied in detail, our knowledges about similar events over the high Arctic during winter is far from being complete. To fill this knowledge gap, in this study, using high spatiotemporal resolution data from the European Centre for Medium-Range Weather Forecasts Reanalysis, version 5 (ERA5), we seek to address the following questions: (1) What are the characteristics of extreme warming events in ERA5, in terms of duration, frequency and temporal clustering? (2) How does the surface energy budget evolve during the development of these events? And what is the dominant energy budget term in driving these events? (3) What are the favorable large-scale circulation patterns driving these events? (4) What roles do ARs play in the initiation of these events in particular?

This paper is structured as follows. Section 2 describes the data and the AR detection algorithm used. In section 3, we first show the characteristics of Arctic extreme warming events, in terms of spatial distribution, duration and occurrence frequency. We then investigate the driving mechanisms of these events from the surface energy budget and large-scale circulation perspectives. Attentions are given to those events with very short or very long duration. As will be shown, the large-scale circulation associated with these events exhibits typical patterns that favor the intrusion of moisture into the Arctic. We thus further quantify the role of ARs in driving or intensifying these events. Lastly, the trends of Arctic extreme warming events are also explored. In section 4, we conclude by giving a brief summary of the major findings and a discussion on some limitations of this study.

2 Methods

2.1 Definition of extreme high Arctic warming events identified in observational dataset

Case studies based on in-situ buoy observations have been conducted to examine the characteristics and drivers of winter extreme warming events over the high Arctic (Moore, 2016; Graham et al., 2017). To facilitate direct comparison with previous case studies, here, extreme warming events are defined as those events with 2-meter air temperature (T2m) over a grid point reaching or exceeding 0℃ over the high Arctic that covers the regions poleward of 80°N. We focus on the winter season (December to February or DJF). The event onset is defined as the time when the T2m first reaches or exceeds 0℃, and the event is considered to end at the time when the T2m first drops below 0℃. The time between the onset and termination is considered as the duration of the event. It is possible that T2m can rise to or above 0℃ within a few hours following the termination of a previous warming event over the same grid point. When such situation occurs, it is likely that both warming events are driven by the same weather system. To test how sensitive the results are to these situations, we impose a 24-hour or

https://doi.org/10.5194/egusphere-2023-2018
Preprint. Discussion started: 20 September 2023

48-hour interval requirement between the termination of an event and the onset of a following event over the same grid point. We found that the results are very similar regardless of whether this additional constraint is imposed or not (not shown). For simplicity, the results being presented in this study are obtained without imposing this constraint.

Results based on previous case studies seem to suggest that these warming events tend to be short-lived, usually with a duration shorter than a few hours. To examine the spatiotemporal characteristics of these warming events in detail, we thus employ hourly data from the fifth generation European Centre for Medium-Range Weather Forecasts reanalysis (ERA5; Hersbach et al., 2020), with a spatial resolution of $0.25^{\circ} \times 0.25^{\circ}$. Previous studies suggest that, compared to in-situ observations, ERA5 exhibits a warm bias in wintertime Arctic surface air temperature (Graham et al., 2019). However, a recent study points out that the warm bias in ERA5 may be state-dependent, with a positive bias found under radiatively clear condition and a negative bias under opaquely cloudy condition (Herrmannsdörfer et al., 2023). Further research is needed to evaluate the performance of ERA5 under extreme warming conditions over the Arctic. Nevertheless, the warming events defined in this study represent very extreme conditions over the high Arctic during winter. The results presented here thus bear significance to our understanding of the characteristics and drivers of winter extreme warming events over the high Arctic.

All anomalies presented in this study are obtained by first removing the seasonal cycle, which is defined based on the period of 1979-2021 for each calendar day using the 31-day running mean data. The Arctic has experienced amplified warming in the past four decades. To exclude the effects of the decadal warming trend, the anomalies of T2m, downward longwave radiation (DLW), integrated water vapor transport (IVT), latent heat flux (LHF), sensible heat flux (SHF), and integrated water vapor (IWV) are further detrended after removing the seasonal cycle. Similarly, the linear trends are based on the period of 1979–2021 for each calendar day using the 31-day running mean of the de-seasonalized data.

2.2 AR detection Algorithm

We use the IVT-based AR detection algorithm developed by Guan and Waliser (2019). This algorithm is an updated version of the original AR detection algorithm, documented in Guan and Waliser (2015), which is one of the earliest and most popular automated AR detection algorithms in the AR community. In addition, it is recommended by the Atmospheric River Tracking Method Intercomparison Project (ARTMIP) for AR research over the high latitudes (Rutz et al., 2019). Notable common criteria employed by both algorithms are as follows: (1) a seasonally and regionally dependent 85^{th} percentile of the IVT magnitude or 100 kg m^{-1} s^{-1}, whichever is larger, is used as the threshold to identify contiguous regions of enhanced IVT ("object"); (2) to ensure coherence, at least half of the grids within the identified object need to have a IVT direction within 45° of the object mean IVT direction; (3) the object mean poleward IVT exceeds 50 kg m^{-1} s^{-1}; lastly (4) the detected object is longer than 2000 km and with a length-to-width ratio exceeding two. Compared to the original algorithm, the updated algorithm includes several major refinements: (1) iterative thresholds are used to increase the chance of an "object" to be detected as AR. In this study, five iterative thresholds are used: 85^{th}, 87.5^{th}, 90^{th}, 92.5^{th} and 95^{th}; (2) improvements are also made on the identification of the AR axis that helps to better characterize the AR length and orientation; (3) the function of tracking of individual ARs across space and time is enabled. By the time when ARs reach the Arctic, they are usually near the end of their

https://doi.org/10.5194/egusphere-2023-2018
Preprint. Discussion started: 20 September 2023

life cycle. Following Mattingly et al. (2018), the length requirement for a detected AR is thus relaxed from 2000 km to 1500 km.

The zonal and meridional components of the IVT vector are calculated by vertically integrating the moisture flux at 1000, 850, 700 and 500 mb following:

$$zonal\ IVT = \frac{1}{g}\int_{1000}^{500} uqdp$$

$$meridional\ IVT = \frac{1}{g}\int_{1000}^{500} vqdp$$

where g is the gravitational acceleration, u is the zonal and v is the meridional wind component, and q is specific humidity. Because using hourly data with the original spatial resolution as input to the AR detection algorithm is computationally too expensive, only data at 00, 06, 12, and 18 UTC are used for AR detection. Furthermore, we bi-linearly regrid the data to $1^\circ \times 1^\circ$ before calculating IVT. The generated AR statistics are then mapped back to the original resolution ($0.25^\circ \times 0.25^\circ$) using the nearest neighbour method.

3 Results

3.1 Characteristics of the high Arctic extreme warming events

Over most of the high Arctic, winter mean T2m is generally below -20 ℃, with the exception found over a small region near 80°N of the Atlantic sector (Fig. 1a). The mean T2m there can reach as high as -13℃. Given such severe cold conditions over the wintertime high Arctic, temperature above 0℃ indeed represents an extreme condition over there. By examining the maximum hourly T2m of all the winter months (December to February) from 1979 to 2021, we found that only regions over the Atlantic sector ever experienced T2m above 0℃ (Fig. 1b), which is consistent with the fact that the Atlantic sector serves as the major pathway for moisture and heat transport into the Arctic (Dufour et al., 2016). The Pacific sector, as another important pathway for moisture and heat transport into the Arctic, has never been warm enough to break 0℃ over 1979-2021, although the winter maximum hourly T2m reached as high as about -1℃. Therefore, we focus on the Atlantic sector from now on.

Consistent with the buoy in-situ observations, these warming events tend to be short-lived, with about 70% and 90% of the events lasting shorter than half a day and one day, respectively (Fig 2c). On average, these events lasted for 11.55 hours. The most long-lasting events are found over the regions close to 80°N between 0°-30°E, with a mean duration of about 16 hours (Fig. 2a). Over this region, those extreme long-lasting events, which are defined as events with duration longer than the local 95th percentile duration, can last longer than two days (Fig. 2b). Moving away from this region, the mean duration drops gradually. Over regions eastward of about 60°E and poleward of about 85°N, the mean duration is shorter than five hours. Over those regions, even the extreme long-lasting events tend to last less than 10 hours, further confirming the short-lived nature of these events over the winter high Arctic observed on buoys.

https://doi.org/10.5194/egusphere-2023-2018
Preprint. Discussion started: 20 September 2023

In addition to being short-lived, these events also occurred very rarely over the winter high Arctic. Regions with mean seasonal occurrence frequency greater than one can only be found over a confined region near 80°N between 0°-30°E (Fig. S1a). Moving away from this region, the occurrence frequency decreases dramatically and becomes less than one over most of the regions. When only those winters with at least one event occurred are considered, the mean occurrence frequency over most regions only increase slightly to 1-2 events per season (Fig. S1b). Besides being rare, by examining the time interval between termination of an event and the onset of the subsequent event for those winters with at least two events occurring over a grid point, we found that these events tend to exhibit some degree of temporal clustering (Fig. 3). About 80% of the events reoccurred in less than five days (Fig. 3a). Over those regions where the mean seasonal occurrence frequency is less than one, the mean time interval in between events is usually less than two days, suggesting that these events tend to occur back-to-back (Fig. 3b). These results suggest that the preconditioning by the previous events likely plays an important role for the initiation of the subsequent events.

3.2 Surface energy budget associated with the high Arctic extreme warming events

It is found that enhanced DLW plays an important role for Arctic warming during winter (Park et al., 2015; Woods and Caballero, 2016; Murto et al., 2023). To investigate whether DLW also plays a role in the extreme warming events defined in this study, we examine the anomalies of the surface energy budget terms when the T2m >= 0℃. As shown in Fig. 4, when T2m >= 0℃, the atmosphere above is anomalously moist, with IWV anomalies exceeding 4 kg m^{-2} nearly everywhere (Fig. 4b). Regional IWV anomalies can reach up to about 9 kg m^{-2}. With the winter IWV climatology being less than 3.5 kg m^{-2} nearly everywhere over the Atlantic sector in the high Arctic (not shown), such moistening of the atmosphere represents 100-300% increases in the IWV and is most likely achieved by intense moisture intrusions from the lower latitudes. Consistent with the moistening of the atmosphere, DLW anomalies also increase substantially everywhere (Fig. 4c). The enhancement of the DLW anomalies increases with latitude and can reach up to about 130 W m^{-2} poleward of 85°N. The spatial pattern of the DLW anomalies corresponds well with that of the IWV anomalies, suggesting the importance of enhanced IWV in inducing the anomalous DLW. Over regions close to 80°N, the magnitude of DLW anomalies is relatively weaker. However, the downward turbulent heat flux (THF) anomalies, especially SHF, are substantially intensified (Fig. 4d, e). Climatologically, the THF over these regions is upward, with magnitudes reaching more than 100 W m^{-2}, due likely to the partially open ocean underneath (Fig. S2). During extreme warming events, the strong advection of both moisture and heat in the lower atmosphere (Fig. 4b, f) likely results in the reversal of the vertical temperature gradient, leading to a strong suppression of the upward THF. In contrast to the spatial pattern of DLW anomalies, the SHF anomalies weaken with latitude. Compared to DLW and SHF, downward LHF anomalies are substantially weaker (Fig. 4e), with the magnitude decreasing with latitude and even a reversed sign over the most north-western regions. The anomalous upward LHF over this region is likely caused by the rapid cold and dry advection shortly after the onset of warming events, resulting in a reversal of the moisture gradient and overall weak temperature advection over the region (Fig. 4f). The patterns of these surface energy budget terms suggest that the winter warming events over the high Arctic can be categorized into two types: (1) the DLW dominance type, which usually occurs

https://doi.org/10.5194/egusphere-2023-2018
Preprint. Discussion started: 20 September 2023

poleward of about 83°N, and (2) the SHF dominance type, which occurs over the lower latitude regions near 80°N. These results are consistent with Murto et al., (2023) who examines the wintertime high Arctic extreme surface energy budget anomalies and finds that DLW plays an increasingly more important role as events move further into the Arctic.

Next, we examine the temporal evolution of the anomalous surface energy budget for the warming events (Fig. 5). Even nine days before the onset of the extreme warming events, T2m is already 3-4 ℃ higher than normal (Fig. 5a). This is likely because these warming events occur more often during warm winters. The background temperature over the Atlantic sector under which these events occur is thus anomalously warm. Indeed, the occurrence frequency of the events correlates significantly with the winter mean T2m over the Atlantic sector of the Arctic (or the entire Arctic), with a correlation coefficient of about 0.64 (0.61). Consistent with the warm anomalies, both IWV and DLW show positive anomalies. These results suggest that a warm and moist winter favours the occurrence of warming events. About four days prior to the onset of the events, T2m, all surface energy budget terms, warm advection and IWV start to climb and peak at around the onset of the events. Both the SHF and DLW play comparable roles in driving the events, with SHF having a slightly larger magnitude. Following the onset of the events, while the other terms drop more gradually, warm advection ceases immediately and shifts to weak cold advection afterwards, implying the passage of cold fronts.

To understand what determines the duration of the events, we further divide the warming events into short duration events, defined by duration <= the 5th percentile of the duration of all events (1 hour), and long duration events, defined by duration >= the 95th percentile of the duration of all events (40 hours). The long duration events only occur equatorward of 85°N while the short duration events can be found both poleward and equatorward of 85°N. As shown above, extreme warming events can be divided into the DLW dominated (poleward of ~83°N) and SHF dominated (equatorward of ~83°N) ones. We thus further divide the short duration events into those occurring poleward of 85°N and equatorward of 83°N to maximize the differences between these two types of events. Since the composites for all the events are dominated by the events with relatively short duration over lower latitude regions, the temporal evolution of T2m, surface energy budget terms, temperature advection and IWV for the short duration events equatorward of 83°N are very similar to those for all the events (Fig. 5c, d vs Fig. 5a, b). For the short duration events poleward of 85°N, the anomalies of T2m, DLW, SHF and IWV start to increase about six days prior to the onset of the events, suggesting that more persistent weather patterns are required to initiate the warming events poleward of 85°N (Fig. 5e, f). Indeed, these events are dominated by the DLW anomalies, with their magnitude being twice those of the SHF anomalies. Following the onset of the events, all quantities drop sharply. The anomalies of SHF and LHF even reverse sign and the warm advection prior to the onset of the events shifts to strong cold advection. Contrary to the short duration events poleward of 85°N, the long duration events are dominated by SHF anomalies, with their magnitude, in this case, being twice those of the DLW anomalies (Fig. 5g). The anomalies did not increase until about two days prior to the onset of the events. Unlike the short duration events, all anomaly terms remain elevated for a prolonged period after the onset of the events, and then gradually level off (Fig. 5g, h)

To further investigate the mechanisms that determine the duration of these events, we create anomaly composites for temperature advection, IVT and SLP centred at the grid point where warming events occur. As shown in Fig. 6, the onset of

https://doi.org/10.5194/egusphere-2023-2018
Preprint. Discussion started: 20 September 2023

the short duration events equatorward of 83°N is associated with a high anomaly to their southeast and a low anomaly to their west. This circulation pattern effectively channels moisture and heat into the regions where the warming events occur. Even six days prior to the onset of the events, the high anomaly already appears. A weak warm advection can also be found south of the event regions. As time evolves, the high anomaly deepens, and a low anomaly starts to develop over the west of the events. Concurrent with these changes in the SLP, moisture transport and warm advection intensify over the event regions. Less than one day prior to the onset of the events, a cold advection anomaly develops west of the events and moves over the event regions immediately following the onset of the events, leading to the drop in T2m. By day six after the onset of the events, the SLP dipole pattern mostly vanishes. For the short duration events poleward of 85°N, the SLP anomaly dipole already starts to develop six days prior to the onset of the events (Fig. 7). As time evolves, the dipole pattern intensifies, resulting in a strong SLP gradient over the event regions. Consistent with the presence of the strong SLP gradient, moisture and heat advection enhance greatly compared to the short duration events equatorward of 83°N. Less than one day prior to the onset of the events, a strong cold advection is well developed over the west of the events. It immediately moves over the event regions after the onset of the events, leading to sharp drops in the T2m and other surface energy budget terms. Like the short duration events equatorward of 83°N, the high anomaly southeast of the event regions already starts to develop for the long duration events (Fig. 8). However, at the meantime, a low anomaly can also be found southwest of the event regions. As the events evolve, the high anomaly intensifies while the low anomaly extends northward. This configuration in the dipole pattern leads to sustained moisture and heat advection into the event regions. Unlike the short duration events, the cold advection west of the long-duration event regions never develops, allowing the warm anomalies to persist. These results suggest that the position of the low anomaly relative to the event regions plays a key role in determining the duration of the events. When the low anomaly is located at the west of event regions, cold advection develops and moves over the event regions immediately after the onset of the events, causing the T2m to fall below 0℃. However, when the low anomaly locates at the southwest of the event regions, cold advection never develops, resulting in sustained moisture and heat advection into the event regions, leading to prolonged warm anomalies.

3.3 Large-scale circulation associated with concurrent warming events

The analyses presented so far are all based on warming events occurring at grid-point scale. We next focus on large-scale circulations responsible for driving concurrent warming events over a large area of the Atlantic sector. To do that, we first calculate the total area experiencing warming events at each hourly snapshot. We then identify all the periods with areas experiencing warming events continually greater than one grid point. These periods are defined as a concurrent warming event. The onset of these concurrent warming events is then defined as the time when the area first exceeds zero (one grid point), and the event ends when the area first falls back to zero. It is possible that the termination of one event is followed shortly by the onset of a subsequent event. Under such a situation, these two concurrent warming events are likely influenced by the same large-scale circulation pattern. We thus impose a constraint that the time interval between two consecutive events needs to be longer than five days. Otherwise, the subsequent event will be discarded in our analysis of large-scale circulations. Lastly, to

https://doi.org/10.5194/egusphere-2023-2018
Preprint. Discussion started: 20 September 2023

focus on the most intense events, only those events with a peak area larger than 5×10^{10} m^{-2} are retained for analyses. There are a total of 96 events that satisfy these criteria. As shown in Fig. 9 (1st column), even four days prior to the peak of the events (day 0), when the total area of warming events reaches maximum, a high SLP anomaly and a low SLP anomaly start to appear over the northwest Eurasia and west Greenland, respectively. As time evolves, the dipole pattern intensifies, and the low anomaly also moves poleward. The anomalous dipole reaches maximum magnitude during the peak of the events and channels large amount of moisture into the Arctic. Four days after the peak of the events, the dipole mostly dissipates.

To gain a more detailed understanding on the spatiotemporal evolution of the large-scale circulation, we apply a K-means clustering method to the spatiotemporal evolution of all 96 events from six days prior to and after the peak of the events. We varied the numbers of clusters ranging from two to four. Three clusters are identified, which give a good balance between the numbers of events in each cluster and sufficient representation of the large-scale circulation patterns. The first cluster features a strong dipole pattern in the SLP anomalies, with a high over northwest Eurasia and a low over Greenland (2nd column in Fig.9). As time evolves, the low SLP anomaly intensifies and propagates into the Arctic and then dissipates over the Laptev Sea, while the high SLP anomaly remains relatively stationary. The second cluster exhibits a strong and persistent high SLP anomaly over northern Eurasia, while the low SLP anomaly is very weak (3rd column in Fig. 9). As time evolves, the low SLP anomaly moves poleward and dissipates rapidly over the Beaufort Sea. Contrary to the second cluster, the high SLP anomaly in the third cluster is very weak and short-lived (4th column in Fig. 9). This cluster is dominated by a low anomaly over Greenland. Unlike the other two clusters, the low SLP anomaly predominantly exhibits a westward movement. These results suggest the importance of blockings for steering cyclones into the Arctic and are consistent with previous studies on the roles of blockings in transporting moisture and heat into the Arctic (Murto et al., 2022; Papritz et al., 2022; Papritz, 2020; Papritz and Dunn-Sigouin, 2020).

Different spatial patterns of the large-scale circulation can result in different impacts (Fig. 10). Compared to the peak time of the T2m anomaly composite of all the events, the first cluster, which is dominated by a strong dipole pattern of SLP anomalies, shows an overall stronger warming over the Atlantic sector (Fig. 10b). However, the area with significant warming is slightly smaller than that based on all the events. The warming anomalies over the Atlantic sector based on the second cluster, which is dominated by the high SLP anomaly, are comparable to the composite of all the events, but it exhibits the largest spatial extent compared to those based on all the events and the other two clusters (Fig. 10c). Lastly, the warm anomaly based on the third cluster, which is dominated by the low SLP anomaly, exhibits the weakest warming over the Atlantic sector, and the spatial extent of the warming anomaly also is confined over the Atlantic sector only (Fig. 10d). Therefore, the presence of the high SLP anomalies or blockings are important in determining both the magnitude and spatial extent of the warm anomalies. These results further imply that the persistence of the blockings over the northwest/northern Eurasia can lead to sustained moisture and heat advection into the Arctic. This, in turn, can precondition the ambient in such a way that once a weather system, such as a cyclone, gets steered into the Arctic, it readily triggers the occurrence of the warming events.

Previous studies have shown that such a dipole pattern in the SLP anomalies is ideal for moisture intrusions or ARs moving into the Arctic (Wang et al., 2020; Park et al., 2015; Woods and Caballero, 2016; Papritz et al., 2022; Papritz and Dunn-

https://doi.org/10.5194/egusphere-2023-2018
Preprint. Discussion started: 20 September 2023

Sigouin, 2020). Indeed, we found that, during the peak time of these concurrent warming events, the AR occurrence frequency, defined as the fraction of time when a grid point is under AR conditions, increases substantially (Fig. 10e-h). The AR frequency can even exceed 30%. With the winter climatological AR frequency ranging from about 0.5-2.5% over the region, this represents an over 10-fold increase in AR frequency. Notably, cluster one, which corresponds to the strong dipole pattern in SLP, is most effective in driving ARs into the Arctic, while cluster three, which corresponds to the low-pressure dominated pattern in SLP, is least effective in driving ARs into the Arctic.

3.4 Roles of ARs in driving the warming events

The above analyses suggest that a strong moisture and heat transport by ARs likely plays roles in driving the warming events. To better quantify this role of ARs, we first examine the surface energy budget during AR days (Fig. 11). Here, AR days experienced over any grid point are defined as those days with at least one 6-hourly time at 00, 06, 12 or 18 UTC under AR condition. During AR days, the surface is anomalously warm, with T2m anomalies exceeding 10℃ nearly everywhere (Fig. 11a). Concurrently, the atmosphere is anomalously moist, with IWV anomalies above 3 kg m^{-2} over most of the area (Fig. 11b). ARs also lead to ubiquitous warm advection (Fig. 11f). Both the sensible heat and latent heat transported by ARs into the Arctic lead to enhanced DLW anomalies, with a magnitude exceeding 60 W m^{-2} nearly everywhere (Fig. 11c). ARs also lead to downward anomalies in both the SHF and LHF, especially over the regions only partially covered by sea ice near 80°N (Fig. 11d, e). These results confirm that ARs indeed have a strong warming effect over the high Arctic during winter.

To show the tight connection more explicitly between ARs and the warming events, Fig. 12a shows the fraction of the warming events which occurs during AR days. Equatorward of about 83°N where the background temperature is relatively warm, ARs are not the only direct driver for warming events. There is still a nonnegligible fraction of events that are driven by other weather disturbances. However, the role of ARs becomes increasingly important as the warming events occur over more poleward regions. Poleward of about 83°N, the fraction of warming events that occur during AR days reaches 100%. Further examining the temporal evolution of IVT for the warming events reveals that IVT usually peaks two to three hours prior to the onset of the events (Fig. S3). The results here thus suggest that, for a large fraction of the regions where warming events can occur, ARs are the only weather system capable of triggering the occurrence of the warming events. Climatologically, the fraction of time with T2m above zero is very close to zero nearly everywhere, except over a small region near 80°N and between 0°-30°E where the fraction can exceed 6% (Fig. 12b). However, if only AR days are considered, the fraction of time with T2m above zero increases substantially (Fig. 12c). By defining the ratio of the fraction of time with T2m above zero during AR days to that of all days as the risk ratio, we can see that ARs increase the risk of warming events dramatically, ranging from about 10 times more likely over lower latitude regions to about 50 times more likely over higher latitude regions (Fig. 12d). ARs are thus likely the key direct driver of the warming events over the high Arctic during winter.

An in-situ observed extreme warming event happened near the end of 2015 and over regions close to the pole (Moore, 2016). If we focus on the regions poleward of 85°N, there are only nine days when warming events occurred over at least one grid point of the regions from 1979 to 2021. ERA5 successfully simulates the occurrence of the warming event during 12/29/2015-

https://doi.org/10.5194/egusphere-2023-2018
Preprint. Discussion started: 20 September 2023

12/30/2015. For all these nine days, ARs can be found intercepting the 85°N latitude over 15°W-60°E for at least one 6-hourly time step of each day, which are defined as AR deep intrusion days, suggesting that all these events are driven directly by ARs. Compared to the AR deep intrusion days without warming events occurring poleward of 85°N, those deep intrusion days with warming events found poleward of 85°N exhibit a much more intense filament of IVT (Fig. 13a vs 13b). The IVT filament also penetrates deeper into the high Arctic. In line with the stronger IVT, the SLP dipole also intensifies, with the low center locating more poleward. During deep intrusion days, the daily IVT averaged over regions poleward of 85°N and between 15°W-60°E increases substantially from the climatological daily mean of ~25 to ~78 kg m^{-1} s^{-1}. Out of the ten (five) highest daily IVT averaged over the defined region, eight (five) of them are associated with warming events occurring poleward of 85°N, further confirming the extreme nature of these warming events.

3.5 Trends of extreme warming events

In the past four decades, winter mean T2m poleward of 80°N has been increasing significantly at a rate of 0.8 ℃ $decade^{-1}$ (Fig. 14a). Consistent with the overall climate warming, both the winter maximum hourly T2m and the mean T2m for those above 0℃ increase significantly at 0.4 ℃ $decade^{-1}$ and 0.09 ℃ $decade^{-1}$, respectively. The slower increase of these extreme T2m events is likely due to the presence of underlying sea ice that imposes a constraint on their warming rates. The background warming also makes the occurrence of the extreme warming events more likely. The event occurrence frequency has been increasing at a rate of 2150 events per season per decade (Fig. 14b). At the same time, they also become more persistent, with the mean duration increased by 1.5 hours per decade. The duration of most long-lasting events each year has increased at an even faster rate of 17.6 hours per decade.

Given the significant increase in both the event frequency and duration, it is natural to ask whether the increases are solely driven by the background warming or changes in AR frequency also play a role. Over the Atlantic sector of the high Arctic, ARs show positive trends over most of the regions in the past four decades (Fig. S4a). However, significant trends are only found over a small region near the pole. Following Ma et al. (2020), we further decompose the trends into a dynamical component, driven by changes in atmospheric circulation, and a thermodynamic component, driven by changes in the moisture field. The decomposition reveals a counterbalancing effect between the two components (Text S1 and Fig. S4). The moistening of the Arctic atmosphere has resulted in a substantial increase in AR frequency, especially over the regions equatorward of 85°N (Fig. S4c and S5a). However, the weakening of winds leads to a reduction in the AR frequency (Fig. S4b and S5b). These two components combined result in insignificant positive trends in the AR frequency over most of the regions. Based on these results, the roles played by changes in AR frequency are likely minor in driving the increase in extreme warming events. Nevertheless, even without any changes in AR frequency, ARs are more likely to induce warming events under a warmer background temperature.

https://doi.org/10.5194/egusphere-2023-2018
Preprint. Discussion started: 20 September 2023

4 Conclusions and Discussions

Using hourly data from ERA5, we perform detailed analyses on the characteristics and drivers of the extreme warming events over the winter high Arctic. Based on ERA5, these events occur predominantly over the Atlantic sector. Except over a small region near 80°N between 0°-30°E, such warming events occur, on average, less frequent than once in each winter. Consistent with in-situ observations (Graham et al., 2017; Moore, 2016), they tend to be short-lived, with a mean duration less than half day. Furthermore, these warming events exhibit some degree of temporal clustering. The temporal clustering identified here could be caused by the clustering of weather systems, as has been found over mid-latitudes for cyclones and ARs (Pinto et al., 2013; Priestley et al., 2017; Fish et al., 2019, 2022). However, further research is still needed to identify whether similar clustering for cyclones and ARs occurs over the high Arctic. By examining their surface energy budget, the warming events can be categorized into two different types: SHF dominance type, which occurs over regions equatorward about 83°N, and the DLW dominance type, which occurs over regions poleward of about 83°N. Notably, long-duration events, which occur over regions near 80°N, are mainly driven by persistent downward SHF anomalies. Composite analysis suggests that the position of the grid point experiencing warming event relative to the low SLP anomaly seems to play a key role in determining the event duration. Short duration events are usually associated with a low SLP anomaly located to its west. This spatial pattern leads to rapid cold advection after the onset of the events and causes T2m to drop below 0℃. When the low SLP anomaly is located at southwest of the grid point with warming event, creating sustained warm advection to the grid point even after the onset of the event, it thus prolongs the event.

The large-scale circulation responsible for the occurrence of warming events over large areas of the Atlantic sector consists of a dipole pattern in the SLP anomalies, with a high anomaly over the northwest Eurasia and a low anomaly over Greenland. This dipole pattern can effectively channel heat and moisture into the high Arctic, resulting in a large-scale warming. K-means clustering applied to the spatiotemporal evolution of these large-scale events further reveals that they mainly consist of three different types of SLP spatial patterns: dipole dominance type, high dominance type, and the low dominance type. By steering cyclones into the high Arctic, the high SLP anomaly or blocking plays an important role in determining both the strength and spatial extent of the concurrent warming events. These large-scale circulations create an ideal environment for moisture intrusions into the Arctic. Using the Guan and Waliser (2019) AR detection algorithm, we show that ARs play a critical role in directly driving the winter high Arctic warming events. Over most of the regions ever experienced extreme warming events, 100% of these events were driven directly by ARs. The chance of having a warming event can even become 50 times higher under AR conditions over some regions than otherwise. ARs are thus potent direct drivers of heat extreme over the high Arctic. In the past four decades, the wintertime mean T2m over the high Arctic has been increasing significantly at a rate of 0.8 ℃ per decade. Concurrent with this rapid warming in the background temperature is the significant increase in both the frequency and the duration of extreme warming events. In contrary to the significant background warming, despite their positive sign, trends in wintertime AR frequency are not yet significant due to the counterbalancing effect of changes in circulation and the moisture field. The increasing trends in the frequency and duration of wintertime extreme warming events are thus likely

https://doi.org/10.5194/egusphere-2023-2018
Preprint. Discussion started: 20 September 2023

driven by the increasingly warming background T2m while the direct contribution from ARs is likely minor. Nevertheless, with continuously amplified warming over the wintertime Arctic and the projected increases in AR activities (Zhang et al., 2021a), the future wintertime high Arctic is expected to witness stronger, more frequent and long-lasting extreme warming events.

The current study does have several limitations. The high spatiotemporal resolution of ERA5 data provides an unprecedented opportunity to investigate the high Arctic wintertime extreme warming events. However, it is known that reanalyses are not real observations. They are produced by numerical models and constrained by limited observations through data assimilation. Biases relative to the actual observations are thus can be expected to exist in reanalysis products (Graham et al., 2019; Huang et al., 2017). Given that in-situ observations over the Arctic, which are used to constrain reanalyses, are sparse, the representations of Arctic climate in reanalyses can be further degraded. This limitation calls for more field campaigns to observe the Arctic atmosphere. In-situ observations for the wintertime extreme warming events and Arctic moisture intrusions or ARs are especially valuable in evaluating the representations of these events in reanalyses. Besides the potential uncertainty associated with the ERA5 dataset used here, AR detection algorithm is another potential source of uncertainties for the results presented in section 3.4. It has been shown that there is a large spread in the detected AR statistics among major global AR detection algorithms participated in ARTMIP (Lora et al., 2020; Rutz et al., 2019). The AR detection algorithm (Guan and Waliser, 2015; 2019) used in this study is one of the very few global AR detection algorithms that can detect noticeable occurrences of ARs over the Arctic. This algorithm is thus recommended by the ARTMIP community for studying high-latitude ARs. For future research focusing on Arctic ARs, intercomparison studies are especially needed to better understand the Arctic AR uncertainties due to AR detection algorithms and/or datasets. The results presented in this study can serve as a good starting point for addressing the limitations discussed above.

References

Amstrup, S. C., DeWeaver, E. T., Douglas, D. C., Marcot, B. G., Durner, G. M., Bitz, C. M., and Bailey, D. A.: Greenhouse gas mitigation can reduce sea-ice loss and increase polar bear persistence, Nature, 468, 955–958, 2010.

Beer, E. and Eisenman, I.: Revisiting the Role of the Water Vapor and Lapse Rate Feedbacks in the Arctic Amplification of Climate Change, J. Clim., 2975–2988, https://doi.org/10.1175/JCLI-D-21-0814.1, 2022.

Binder, H., Boettcher, M., Grams, C. M., Joos, H., Pfahl, S., and Wernli, H.: Exceptional Air Mass Transport and Dynamical Drivers of an Extreme Wintertime Arctic Warm Event, Geophys. Res. Lett., 44, 12,028-12,036, https://doi.org/10.1002/2017GL075841, 2017.

Bintanja, R., van der Wiel, K., van der Linden, E. C., Reusen, J., Bogerd, L., Krikken, F., and Selten, F. M.: Strong future increases in Arctic precipitation variability linked to poleward moisture transport, Sci. Adv., 6, eaax6869, https://doi.org/10.1126/sciadv.aax6869, 2020.

https://doi.org/10.5194/egusphere-2023-2018
Preprint. Discussion started: 20 September 2023

Cohen, J., Screen, J. A., Furtado, J. C., Barlow, M., Whittleston, D., Coumou, D., Francis, J., Dethloff, K., Entekhabi, D., Overland, J., and Jones, J.: Recent Arctic amplification and extreme mid-latitude weather, Nat. Geosci., 7, 627–637, https://doi.org/10.1038/ngeo2234, 2014.

Crawford, A. D., Lukovich, J. V, McCrystall, M. R., Stroeve, J. C., and Barber, D. G.: Reduced sea ice enhances intensification of winter storms over the Arctic Ocean, J. Clim., 35, 3353–3370, 2022.

Dai, A., Luo, D., Song, M., and Liu, J.: Arctic amplification is caused by sea-ice loss under increasing CO2, Nat. Commun., 10, 121, 2019.

Dobricic, S., Russo, S., Pozzoli, L., Wilson, J., and Vignati, E.: Increasing occurrence of heat waves in the terrestrial Arctic, Environ. Res. Lett., 15, 24022, 2020.

Dou, T., Xiao, C., Liu, J., Wang, Q., Pan, S., Su, J., Yuan, X., Ding, M., Zhang, F., Xue, K., and others: Trends and spatial variation in rain-on-snow events over the Arctic Ocean during the early melt season, Cryosph., 15, 883–895, 2021.

Dufour, A., Zolina, O., and Gulev, S. K.: Atmospheric moisture transport to the Arctic: Assessment of reanalyses and analysis of transport components, J. Clim., 29, 5061–5081, 2016.

Fish, M. A., Wilson, A. M., and Ralph, F. M.: Atmospheric river families: Definition and associated synoptic conditions, J. Hydrometeorol., 20, 2091–2108, 2019.

Fish, M. A., Done, J. M., Swain, D. L., Wilson, A. M., Michaelis, A. C., Gibson, P. B., and Ralph, F. M.: Large-scale environments of successive atmospheric river events leading to compound precipitation extremes in California, J. Clim., 35, 1515–1536, 2022.

Ford, J. D., Harper, S., Pearce, T., and Canosa, I. V.: The rapidly changing Arctic and its societal implications, 1–27, https://doi.org/10.1002/wcc.735, 2021.

Gimeno, L., Vázquez, M., Eiras-Barca, J., Sor\'\i, R., Algarra, I., and Nieto, R.: Atmospheric moisture transport and the decline in Arctic Sea ice, Wiley Interdiscip. Rev. Clim. Chang., 10, e588, 2019.

Graham, R. M., Cohen, L., Petty, A. A., Boisvert, L. N., Rinke, A., Hudson, S. R., Nicolaus, M., and Granskog, M. A.: Increasing frequency and duration of Arctic winter warming events, Geophys. Res. Lett., 44, 6974–6983, https://doi.org/10.1002/2017GL073395, 2017.

Graham, R. M., Cohen, L., Ritzhaupt, N., Segger, B., Graversen, R. G., Rinke, A., Walden, V. P., Granskog, M. A., and Hudson, S. R.: Evaluation of six atmospheric reanalyses over Arctic sea ice from winter to early summer, J. Clim., 32, 4121–4143, 2019.

Graversen, R. G. and Burtu, M.: Arctic amplification enhanced by latent energy transport of atmospheric planetary waves, 2046–2054, https://doi.org/10.1002/qj.2802, 2016.

Graversen, R. G. and Langen, P. L.: On the Role of the Atmospheric Energy Transport in 2 3 CO 2 – Induced Polar Amplification in CESM1, J. Clim., 3941–3956, https://doi.org/10.1175/JCLI-D-18-0546.1, 2019.

Guan, B. and Waliser, D. E.: Detection of atmospheric rivers: Evaluation and application of an algorithm for global studies, J. Geophys. Res. Atmos., 120, 12514–12535, 2015.

https://doi.org/10.5194/egusphere-2023-2018
Preprint. Discussion started: 20 September 2023

Guan, B. and Waliser, D. E.: Tracking atmospheric rivers globally: Spatial distributions and temporal evolution of life cycle characteristics, J. Geophys. Res. Atmos., 124, 12523–12552, 2019.

Hegyi, B. M. and Taylor, P. C.: The unprecedented 2016--2017 Arctic sea ice growth season: The crucial role of atmospheric rivers and longwave fluxes, Geophys. Res. Lett., 45, 5204–5212, 2018.

Herrmannsdörfer, L., Müller, M., Shupe, M. D., and Rostosky, P.: Surface temperature comparison of the Arctic winter MOSAiC observations, ERA5 reanalysis, and MODIS satellite retrieval, Elem Sci Anth, 11, 85, 2023.

Hersbach, H., Bell, B., Berrisford, P., Hirahara, S., Horányi, A., Muñoz-Sabater, J., Nicolas, J., Peubey, C., Radu, R., Schepers, D., Simmons, A., Soci, C., Abdalla, S., Abellan, X., Balsamo, G., Bechtold, P., Biavati, G., Bidlot, J., Bonavita, M., De Chiara, G., Dahlgren, P., Dee, D., Diamantakis, M., Dragani, R., Flemming, J., Forbes, R., Fuentes, M., Geer, A., Haimberger, L., Healy, S., Hogan, R. J., Hólm, E., Janisková, M., Keeley, S., Laloyaux, P., Lopez, P., Lupu, C., Radnoti, G., de Rosnay, P., Rozum, I., Vamborg, F., Villaume, S., and Thépaut, J. N.: The ERA5 global reanalysis, Q. J. R. Meteorol. Soc., 146, 1999–2049, https://doi.org/10.1002/qj.3803, 2020.

Huang, Y., Dong, X., Qiu, S., Xi, B., Dolinar, E. K., and Stanfield, R. E.: Quantifying the uncertainties of reanalyzed Arctic cloud and radiation properties using satellite surface observations, J. Clim., 30, 8007–8029, https://doi.org/10.1175/JCLI-D-16-0722.1, 2017.

Hwang, Y. T., Frierson, D. M. W., and Kay, J. E.: Coupling between Arctic feedbacks and changes in poleward energy transport, Geophys. Res. Lett., 38, 1–5, https://doi.org/10.1029/2011GL048546, 2011.

Kapsch, M.-L., Graversen, R. G., and Tjernström, M.: Springtime atmospheric energy transport and the control of Arctic summer sea-ice extent, Nat. Clim. Chang., 3, 744–748, 2013.

Kumar, A., Perlwitz, J., Eischeid, J., Quan, X., Xu, T., Zhang, T., Hoerling, M., Jha, B., and Wang, W.: Contribution of sea ice loss to Arctic amplification, 37, 2–7, https://doi.org/10.1029/2010GL045022, 2010.

Lamjiri, M. A., Dettinger, M. D., Ralph, F. M., and Guan, B.: Hourly storm characteristics along the US West Coast: Role of atmospheric rivers in extreme precipitation, Geophys. Res. Lett., 44, 7020–7028, 2017.

Lavers, D. A. and Villarini, G.: The contribution of atmospheric rivers to precipitation in Europe and the United States, J. Hydrol., 522, 382–390, https://doi.org/10.1016/j.jhydrol.2014.12.010, 2015.

Leung, L. R. and Qian, Y.: Atmospheric rivers induced heavy precipitation and flooding in the western US simulated by the WRF regional climate model, Geophys. Res. Lett., 36, 2009.

Lora, J. M., Shields, C. A., and Rutz, J. J.: Consensus and disagreement in atmospheric river detection: ARTMIP global catalogues, Geophys. Res. Lett., 47, e2020GL089302, 2020.

Ma, W., Chen, G., and Guan, B.: Poleward Shift of Atmospheric Rivers in the Southern Hemisphere in Recent Decades, Geophys. Res. Lett., submitted, https://doi.org/10.1029/2020GL089934, 2020.

Ma, W., Chen, G., Peings, Y., and Alviz, N.: Atmospheric River Response to Arctic Sea Ice Loss in the Polar Amplification Model Intercomparison Project, Geophys. Res. Lett., 48, 1–12, https://doi.org/10.1029/2021gl094883, 2021.

Mattingly, K. S., Mote, T. L., and Fettweis, X.: Atmospheric river impacts on Greenland Ice Sheet surface mass balance, J.

https://doi.org/10.5194/egusphere-2023-2018
Preprint. Discussion started: 20 September 2023

Geophys. Res. Atmos., 123, 8538–8560, 2018.

Moore, G. W. K.: The December 2015 North Pole warming event and the increasing occurrence of such events, Sci. Rep., 6, 1–11, 2016.

Mortin, J., Svensson, G., Graversen, R. G., Kapsch, M.-L., Stroeve, J. C., and Boisvert, L. N.: Melt onset over Arctic sea ice controlled by atmospheric moisture transport, Geophys. Res. Lett., 43, 6636–6642, 2016.

Murto, S., Caballero, R., Svensson, G., and Papritz, L.: Interaction between Atlantic cyclones and Eurasian atmospheric blocking drives wintertime warm extremes in the high Arctic, Weather Clim. Dyn., 3, 21–44, 2022.

Murto, S., Papritz, L., Messori, G., Caballero, R., Svensson, G., and Wernli, H.: Extreme surface energy budget anomalies in the high Arctic in winter, J. Clim., 36, 3591–3609, 2023.

Nash, D., Waliser, D., Guan, B., Ye, H., and Ralph, F. M.: The Role of Atmospheric Rivers in Extratropical and Polar Hydroclimate, J. Geophys. Res. Atmos., 123, 6804–6821, https://doi.org/10.1029/2017JD028130, 2018.

Pan, M. and Lu, M.: East Asia atmospheric river catalog: Annual cycle, transition mechanism, and precipitation, Geophys. Res. Lett., 47, e2020GL089477, 2020.

Papritz, L.: Arctic lower-tropospheric warm and cold extremes: Horizontal and vertical transport, diabatic processes, and linkage to synoptic circulation features, J. Clim., 33, 993–1016, 2020.

Papritz, L. and Dunn-Sigouin, E.: What configuration of the atmospheric circulation drives extreme net and total moisture transport into the Arctic, Geophys. Res. Lett., 47, e2020GL089769, 2020.

Papritz, L., Hauswirth, D., and Hartmuth, K.: Moisture origin, transport pathways, and driving processes of intense wintertime moisture transport into the Arctic, Weather Clim. Dyn., 3, 1–20, 2022.

Park, H.-S., Lee, S., Son, S.-W., Feldstein, S. B., and Kosaka, Y.: The impact of poleward moisture and sensible heat flux on Arctic winter sea ice variability, J. Clim., 28, 5030–5040, 2015.

Parker, C. L., Mooney, P. A., Webster, M. A., and Boisvert, L. N.: The influence of recent and future climate change on spring Arctic cyclones, Nat. Commun., 13, 6514, 2022.

Pinto, J. G., Bellenbaum, N., Karremann, M. K., and Della-Marta, P. M.: Serial clustering of extratropical cyclones over the North Atlantic and Europe under recent and future climate conditions, J. Geophys. Res. Atmos., 118, 12–476, 2013.

Pithan, F. and Mauritsen, T.: Arctic amplification dominated by temperature feedbacks in contemporary climate models, 7, 181–184, https://doi.org/10.1038/NGEO2071, 2014.

Post, E., Bhatt, U. S., Bitz, C. M., Brodie, J. F., Fulton, T. L., Hebblewhite, M., Kerby, J., Kutz, S. J., Stirling, I., and Walker, D. A.: Ecological consequences of sea-ice decline, Science (80-.)., 341, 519–524, 2013.

Previdi, M., Smith, K. L., and Polvani, L. M.: Arctic amplification of climate change: a review of underlying mechanisms, Environ. Res. Lett., 16, 93003, 2021.

Priestley, M. D. K., Pinto, J. G., Dacre, H. F., and Shaffrey, L. C.: Rossby wave breaking, the upper level jet, and serial clustering of extratropical cyclones in western Europe, Geophys. Res. Lett., 44, 514–521, 2017.

Rantanen, M., Karpechko, A. Y., Lipponen, A., Nordling, K., Hyvärinen, O., Ruosteenoja, K., Vihma, T., and Laaksonen, A.:

https://doi.org/10.5194/egusphere-2023-2018
Preprint. Discussion started: 20 September 2023

The Arctic has warmed nearly four times faster than the globe since 1979, Commun. Earth Environ., 3, 1–10, https://doi.org/10.1038/s43247-022-00498-3, 2022.

Rinke, A., Maturilli, M., Graham, R. M., Matthes, H., Handorf, D., Cohen, L., Hudson, S. R., and Moore, J. C.: Extreme cyclone events in the Arctic: Wintertime variability and trends, Environ. Res. Lett., 12, 94006, 2017.

Rutz, J. J., Shields, C. A., Lora, J. M., Payne, A. E., Guan, B., Ullrich, P., O'Brien, T., Leung, L. R., Ralph, F. M., Wehner, M., Brands, S., Collow, A., Goldenson, N., Gorodetskaya, I., Griffith, H., Kashinath, K., Kawzenuk, B., Krishnan, H., Kurlin, V., Lavers, D., Magnusdottir, G., Mahoney, K., McClenny, E., Muszynski, G., Nguyen, P. D., Prabhat, M., Qian, Y., Ramos, A. M., Sarangi, C., Sellars, S., Shulgina, T., Tome, R., Waliser, D., Walton, D., Wick, G., Wilson, A. M., and Viale, M.: The Atmospheric River Tracking Method Intercomparison Project (ARTMIP): Quantifying Uncertainties in Atmospheric River Climatology, J. Geophys. Res. Atmos., 124, 13777–13802, https://doi.org/10.1029/2019JD030936, 2019.

Schröder, D., Feltham, D. L., Flocco, D., and Tsamados, M.: September Arctic sea-ice minimum predicted by spring melt-pond fraction, Nat. Clim. Chang., 4, 353–357, 2014.

Screen, J. A. and Simmonds, I.: The central role of diminishing sea ice in recent Arctic temperature amplification, Nature, 464, 1334–1337, 2010.

Screen, J. A., Deser, C., Smith, D. M., Zhang, X., Blackport, R., Kushner, P. J., Oudar, T., McCusker, K. E., and Sun, L.: Consistency and discrepancy in the atmospheric response to Arctic sea-ice loss across climate models, Nat. Geosci., 11, 155–163, https://doi.org/10.1038/s41561-018-0059-y, 2018.

Serreze, M. C. and Barry, R. G.: Processes and impacts of Arctic amplification: A research synthesis, Glob. Planet. Change, 77, 85–96, 2011.

Serreze, M. C. and Stroeve, J.: Arctic sea ice trends, variability and implications for seasonal ice forecasting, Philos. Trans. R. Soc. A Math. Phys. Eng. Sci., 373, 20140159, 2015.

Serreze, M. C., Gustafson, J., Barrett, A. P., Druckenmiller, M. L., Fox, S., Voveris, J., Stroeve, J., Sheffield, B., Forbes, B. C., Rasmus, S., and others: Arctic rain on snow events: bridging observations to understand environmental and livelihood impacts, Environ. Res. Lett., 16, 105009, 2021.

Singh, H. A., Rasch, P. J., and Rose, B. E. J.: Increased ocean heat convergence into the high latitudes with CO2 doubling enhances polar-amplified warming, Geophys. Res. Lett., 44, 10–583, 2017.

Stroeve, J. and Notz, D.: Changing state of Arctic sea ice across all seasons, Environ. Res. Lett., 13, 103001, 2018.

Stuecker, M. F., Bitz, C. M., Armour, K. C., Proistosescu, C., Kang, S. M., Xie, S.-P., Kim, D., McGregor, S., Zhang, W., Zhao, S., and others: Polar amplification dominated by local forcing and feedbacks, Nat. Clim. Chang., 8, 1076–1081, 2018.

Vavrus, S.: The impact of cloud feedbacks on Arctic climate under greenhouse forcing, J. Clim., 17, 603–615, 2004.

Viale, M., Valenzuela, R., Garreaud, R. D., and Ralph, F. M.: Impacts of atmospheric rivers on precipitation in southern South America, J. Hydrometeorol., 19, 1671–1687, 2018.

Waliser, D. and Guan, B.: Extreme winds and precipitation during landfall of atmospheric rivers, Nat. Geosci., 10, 179–183, https://doi.org/10.1038/ngeo2894, 2017.

https://doi.org/10.5194/egusphere-2023-2018
Preprint. Discussion started: 20 September 2023

Wang, Z., Walsh, J., Szymborski, S., and Peng, M.: Rapid Arctic sea ice loss on the synoptic time scale and related atmospheric circulation anomalies, J. Clim., 33, 1597–1617, 2020.

Woods, C. and Caballero, R.: The role of moist intrusions in winter arctic warming and sea ice decline, J. Clim., 29, 4473–4485, https://doi.org/10.1175/JCLI-D-15-0773.1, 2016.

Zhang, P., Chen, G., Ma, W., Ming, Y., and Wu, Z.: Robust atmospheric river response to global warming in idealized and comprehensive climate models, J. Clim., 34, 7717–7734, https://doi.org/10.1175/JCLI-D-20-1005.1, 2021a.

Zhang, P., Chen, G., Ting, M., Ruby Leung, L., Guan, B., and Li, L.: More frequent atmospheric rivers slow the seasonal recovery of Arctic sea ice, Nat. Clim. Chang., 13, https://doi.org/10.1038/s41558-023-01599-3, 2023.

Zhang, R., Wang, H., Fu, Q., Rasch, P. J., Wu, M., and Maslowski, W.: Understanding the cold season Arctic surface warming trend in recent decades, Geophys. Res. Lett., 48, e2021GL094878, 2021b.

Zhang, X., He, J., Zhang, J., Polyakov, I., Gerdes, R., Inoue, J., and Wu, P.: Enhanced poleward moisture transport and amplified northern high-latitude wetting trend, Nat. Clim. Chang., 3, 47–51, 2013.

Zhu, Y. and Newell, R. E.: A proposed algorithm for moisture fluxes from atmospheric rivers, Mon. Weather Rev., 126, 725–735, https://doi.org/10.1175/1520-0493(1998)126<0725:APAFMF>2.0.CO;2, 1998.

Zou, Y., Rasch, P. J., Wang, H., Xie, Z., and Zhang, R.: Increasing large wildfires over the western United States linked to diminishing sea ice in the Arctic, Nat. Commun., 12, 6048, 2021.

Data Availability

ERA5 data can be found at https://www.ecmwf.int/en/forecasts/dataset/ecmwf-reanalysis-v5

Author Contributions

W.M. conceived the study. W.M. designed the study with contributions from H.W. W.M. performed the analyses and wrote the initial draft of the paper. All authors contributed to interpreting the results, editing, and revising the manuscript.

Competing Interests

At least one of the co-authors is an editor of Atmospheric Chemistry and Physics.

https://doi.org/10.5194/egusphere-2023-2018
Preprint. Discussion started: 20 September 2023

Acknowledgements

This research was supported by the U.S. Department of Energy (DOE), Office of Science, Office of Biological and Environmental Research, Regional and Global Model Analysis program area, as part of the HiLAT-RASM project. This research used resources of the National Energy Research Scientific Computing Center (NERSC), a U.S. DOE Office of Science User Facility operated under Contract No. DE-AC02-05CH11231. The Pacific Northwest National Laboratory (PNNL) is operated for DOE by Battelle Memorial Institute under contract DE-AC05-76RLO1830.

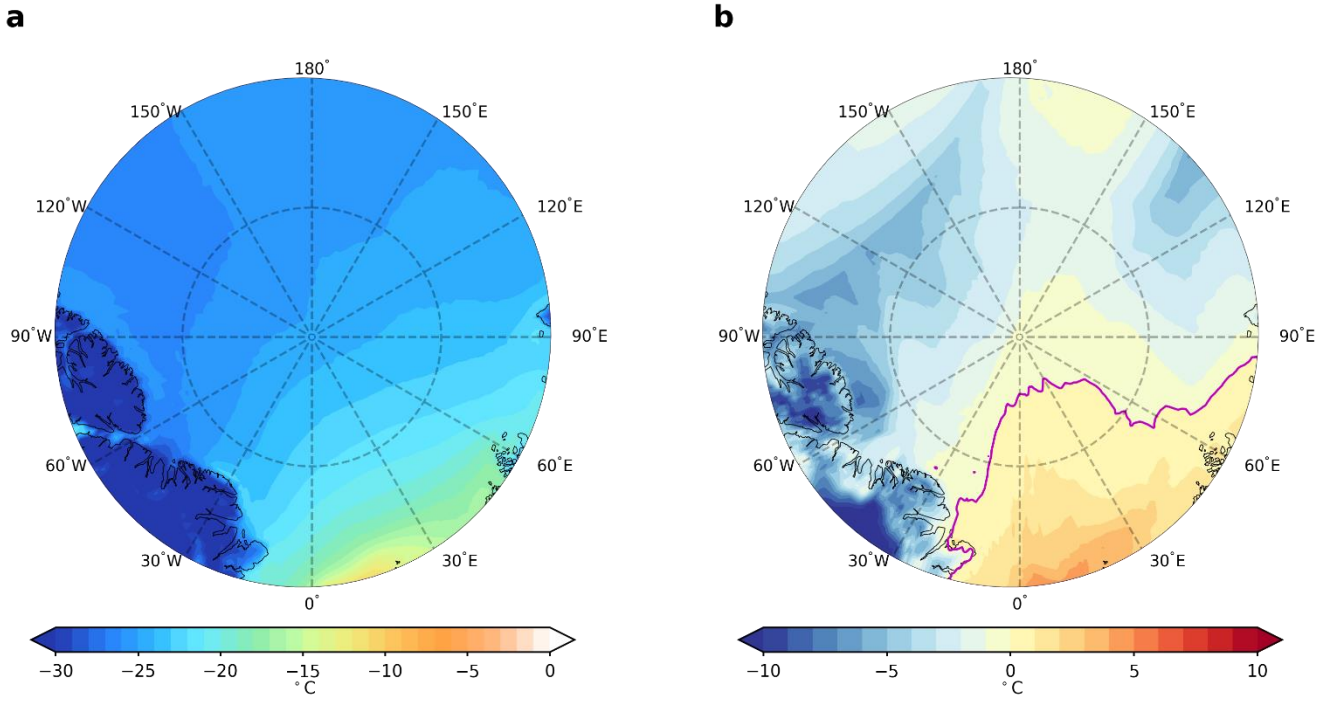

Figure 1. (a) time mean 2-meter air temperature (T2m) and (b) maximum hourly T2m over all winter from 1979 to 2021. The purple line denotes **0**°C.

https://doi.org/10.5194/egusphere-2023-2018
Preprint. Discussion started: 20 September 2023

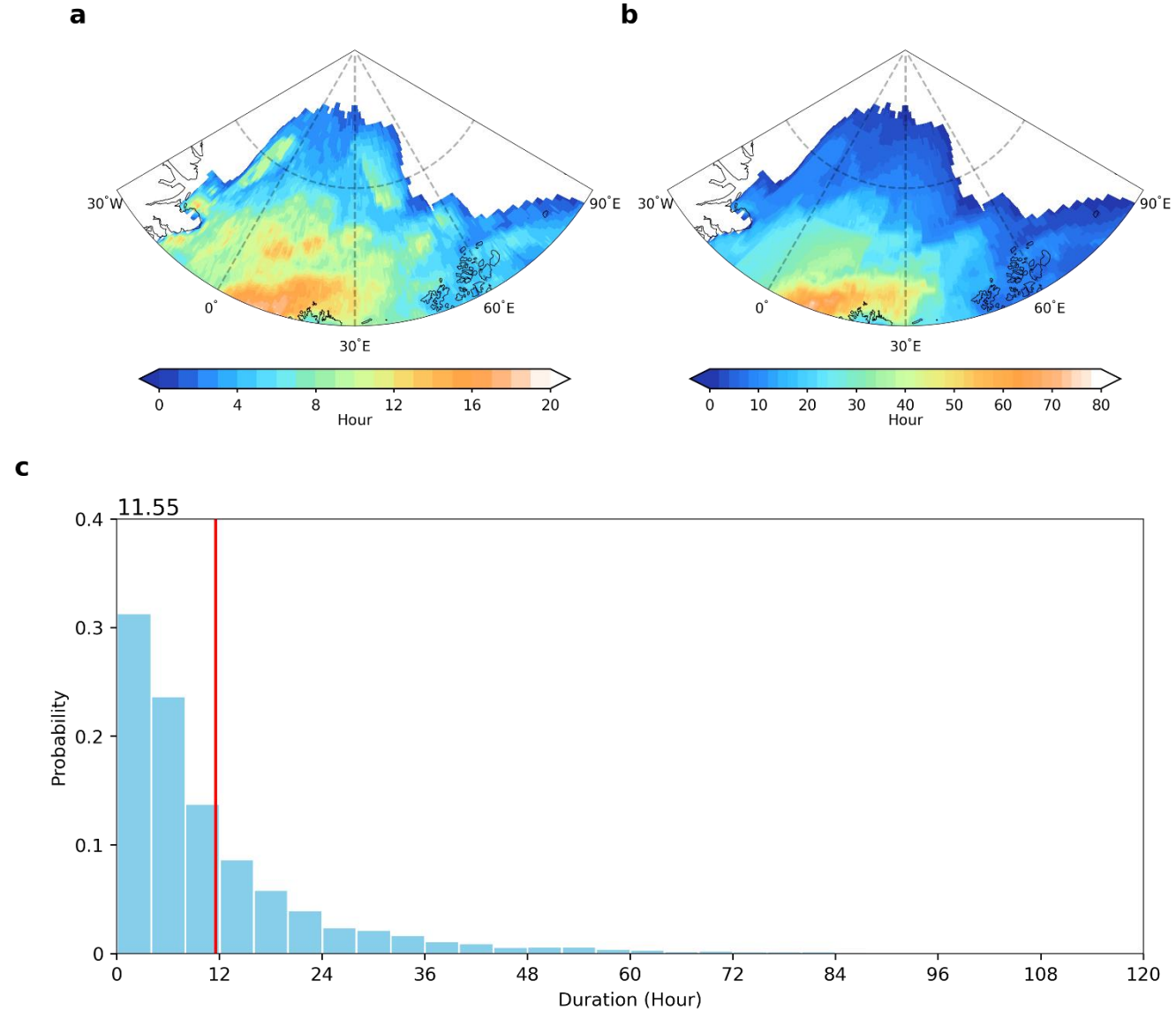

Figure 2. Spatial distribution of the (a) mean duration and (b) extreme duration of the high Arctic warming events. Extreme duration is defined as the local 95th percentile of the duration distribution. (c) Probability density function of the duration distribution for all events happened during winter from 1979 to 2021. The red vertical line in (c) marks the mean of the distribution (11.55 hours).

610

https://doi.org/10.5194/egusphere-2023-2018
Preprint. Discussion started: 20 September 2023

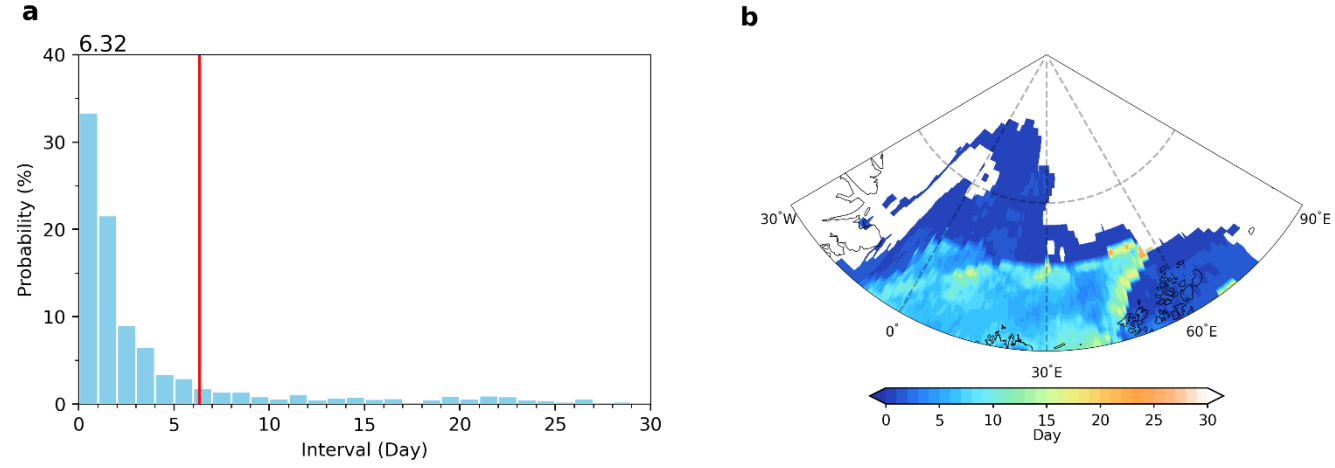

Figure 3. (a) Probability density function of the time interval between the termination of an event and the onset of the following event over the same grid point. (b) Spatial distribution for the mean time interval. The red vertical line in (c) marks the mean of the distribution (6.32 days).

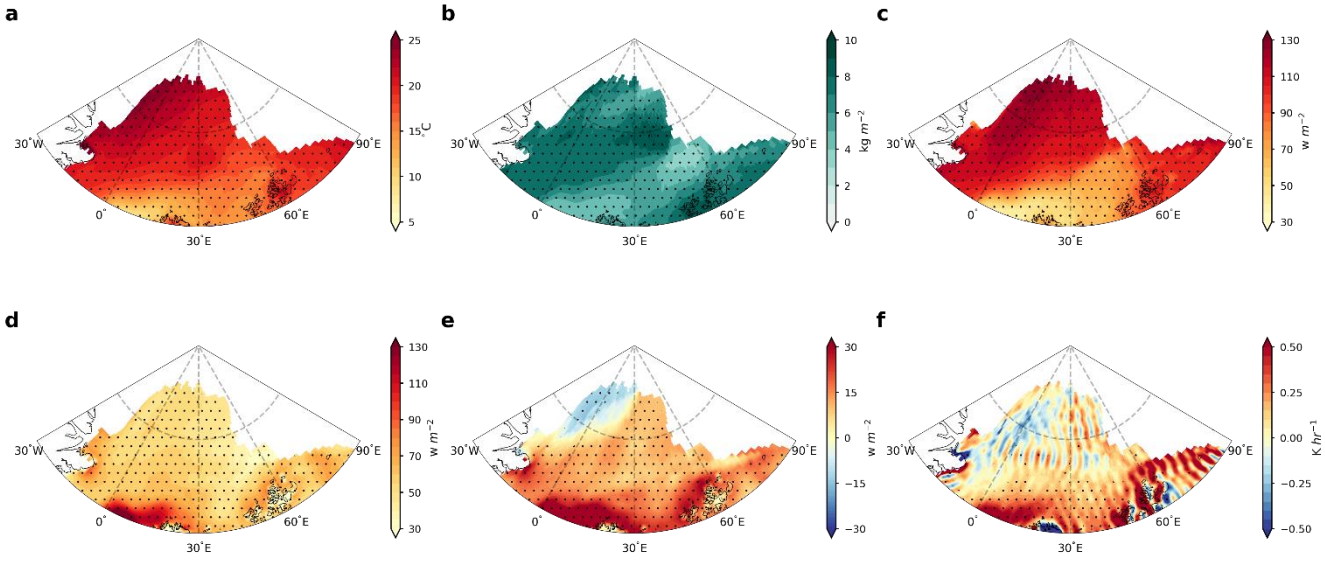

Figure 4. Spatial distribution of the anomalies of (a) T2m, (b) column-integrated water vapor (IWV), (c) downward longwave radiation (DLW), (d) sensible heat flux (SHF), (e) latent heat flux (LHF) and (f) horizontal temperature advection during the warming events. Stippled areas indicate that anomalies are significant at the 0.05 level based on the Student's t-test.

https://doi.org/10.5194/egusphere-2023-2018
Preprint. Discussion started: 20 September 2023

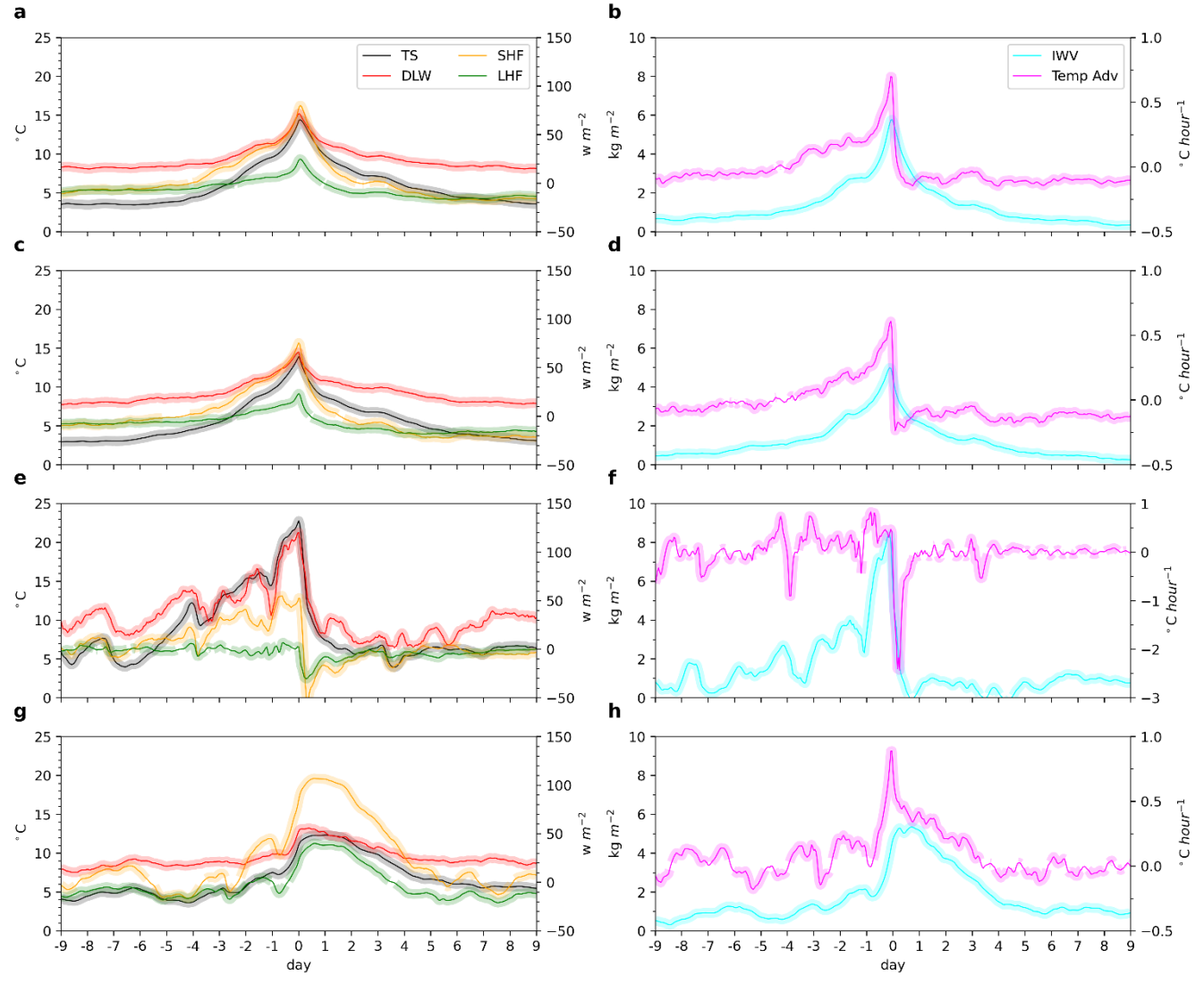

Figure 5. Temporal evolution of the anomalies of T2m, DLW, SHF, LHF, IWV and temperature advection for all the warming events (a, b), short duration events equatorward of 83°N (c, d), short duration events poleward of 85°N (e, f), and long duration events (g, h). The shading indicates that the anomalies are significant at the 0.05 level based on the Student's t-test.

https://doi.org/10.5194/egusphere-2023-2018
Preprint. Discussion started: 20 September 2023

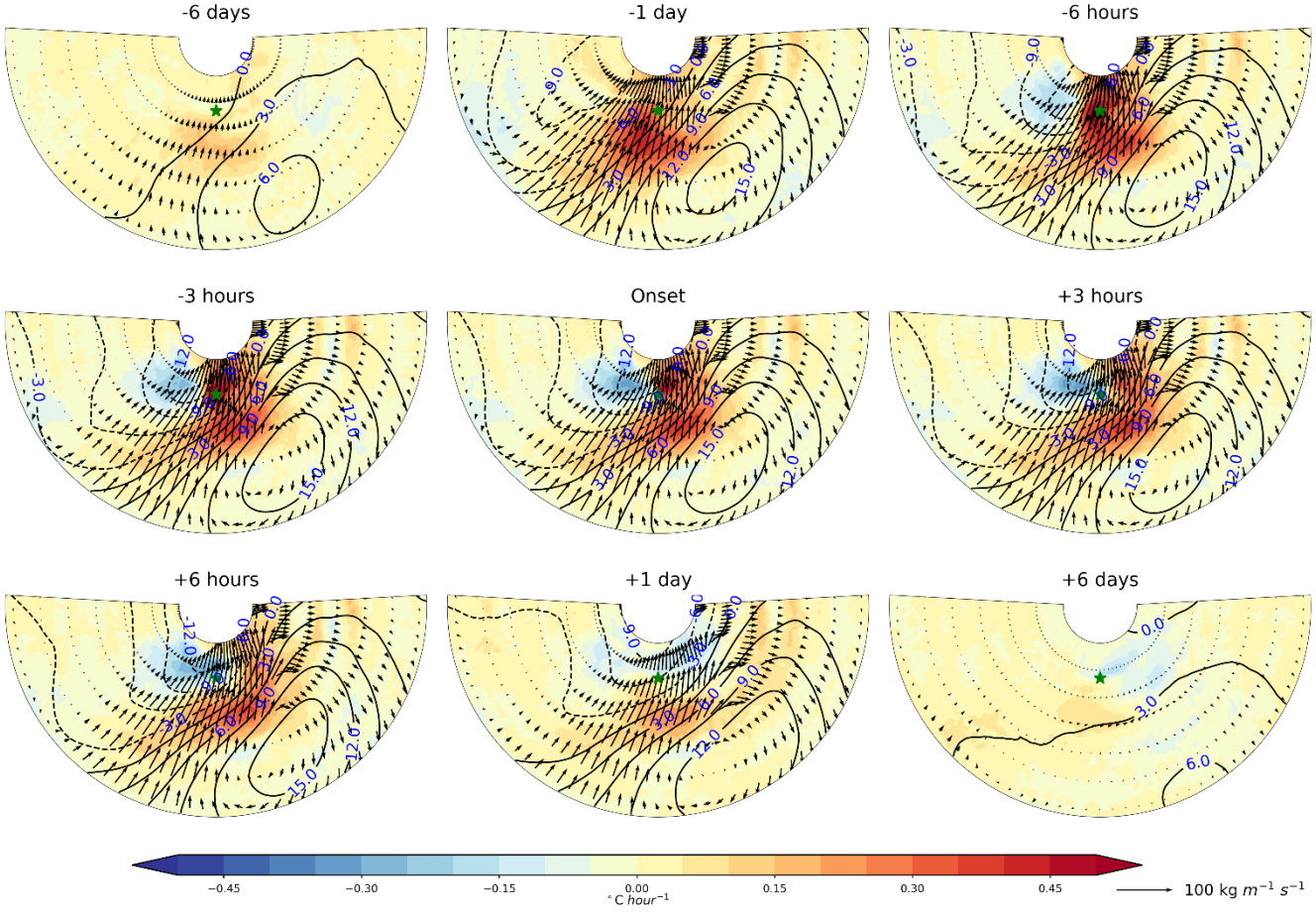

Figure 6. Composites centred at the event grid point for the temporal evolution of integrated water vapor transport (IVT) anomalies (vectors), sea level pressure (SLP) anomalies (lines) and temperature advection anomalies (shading) before, during and after the onset of the short duration warming events equatorward of 83°N. The green star in each panel indicates the grid point where the warming events took place. Regions 5° poleward, 20° equatorward, 100° westward/eastward of the event grid point are included in the composites.

https://doi.org/10.5194/egusphere-2023-2018
Preprint. Discussion started: 20 September 2023

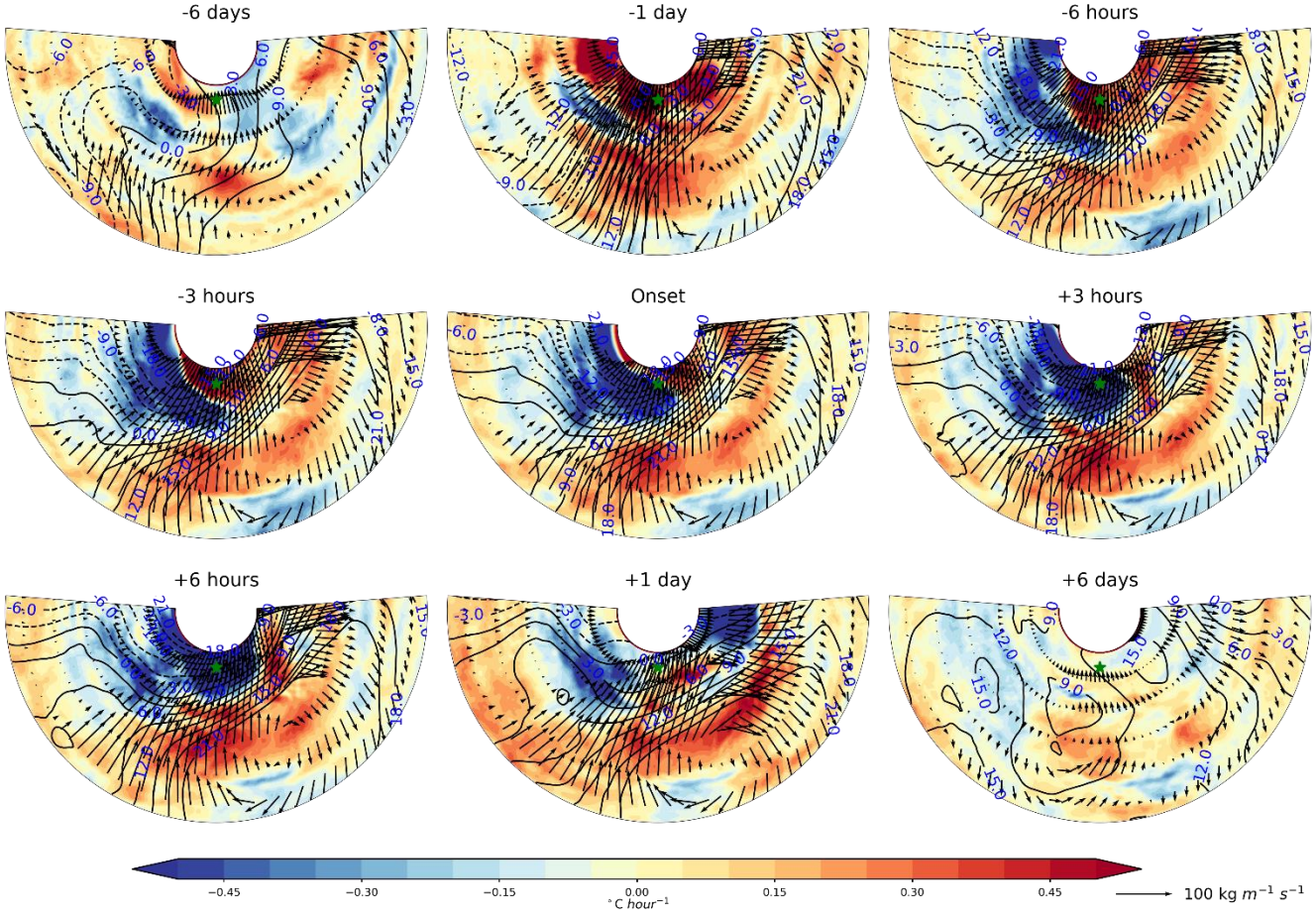

Figure 7. Same as Fig. 6, but for the short duration events poleward of 85°N. Regions 2° poleward, 20° equatorward, 100° westward/eastward of the event grid point are included in the composites.

640

https://doi.org/10.5194/egusphere-2023-2018
Preprint. Discussion started: 20 September 2023

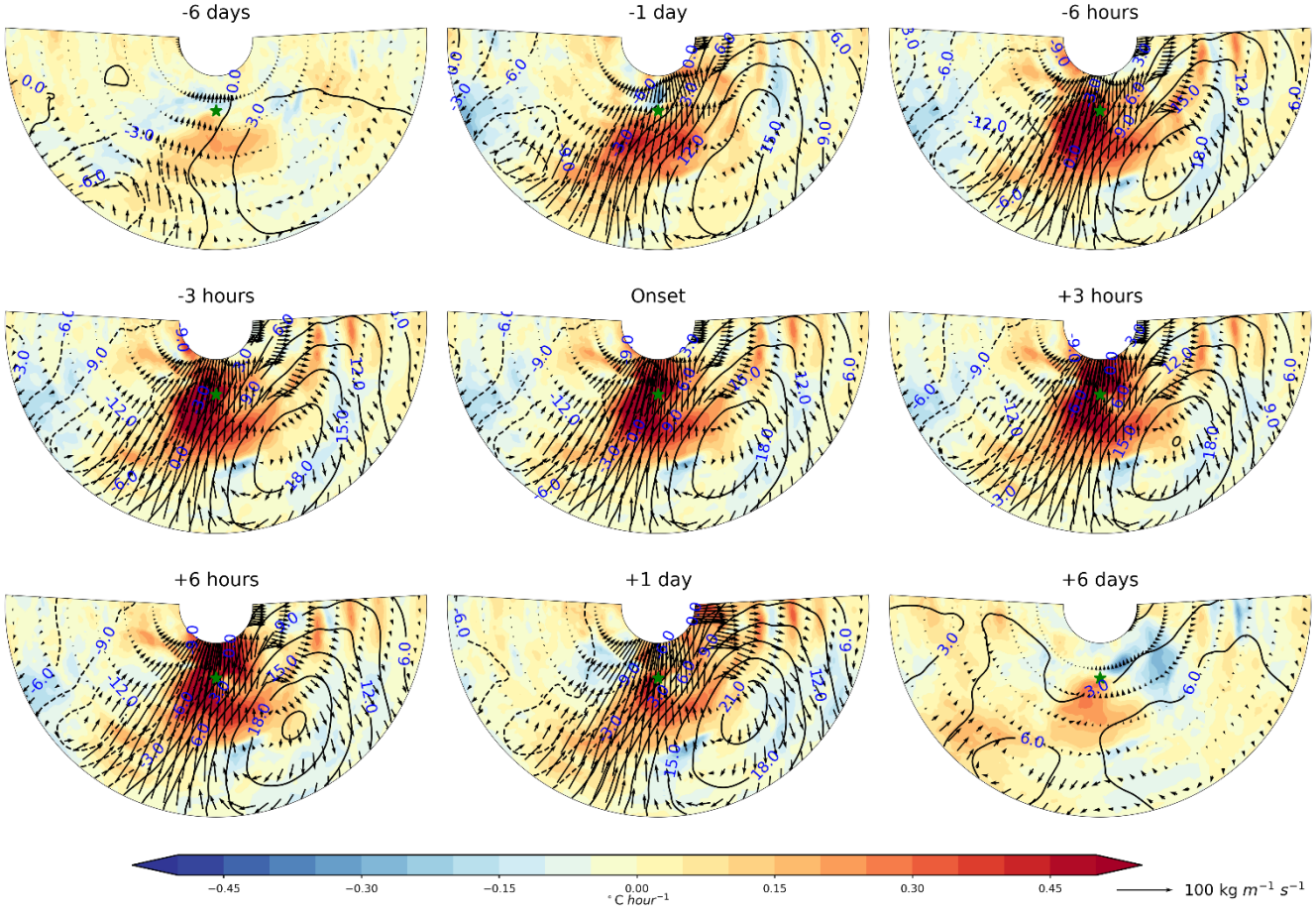

Figure 8. Same as Fig. 6, but for the long duration events.

https://doi.org/10.5194/egusphere-2023-2018
Preprint. Discussion started: 20 September 2023

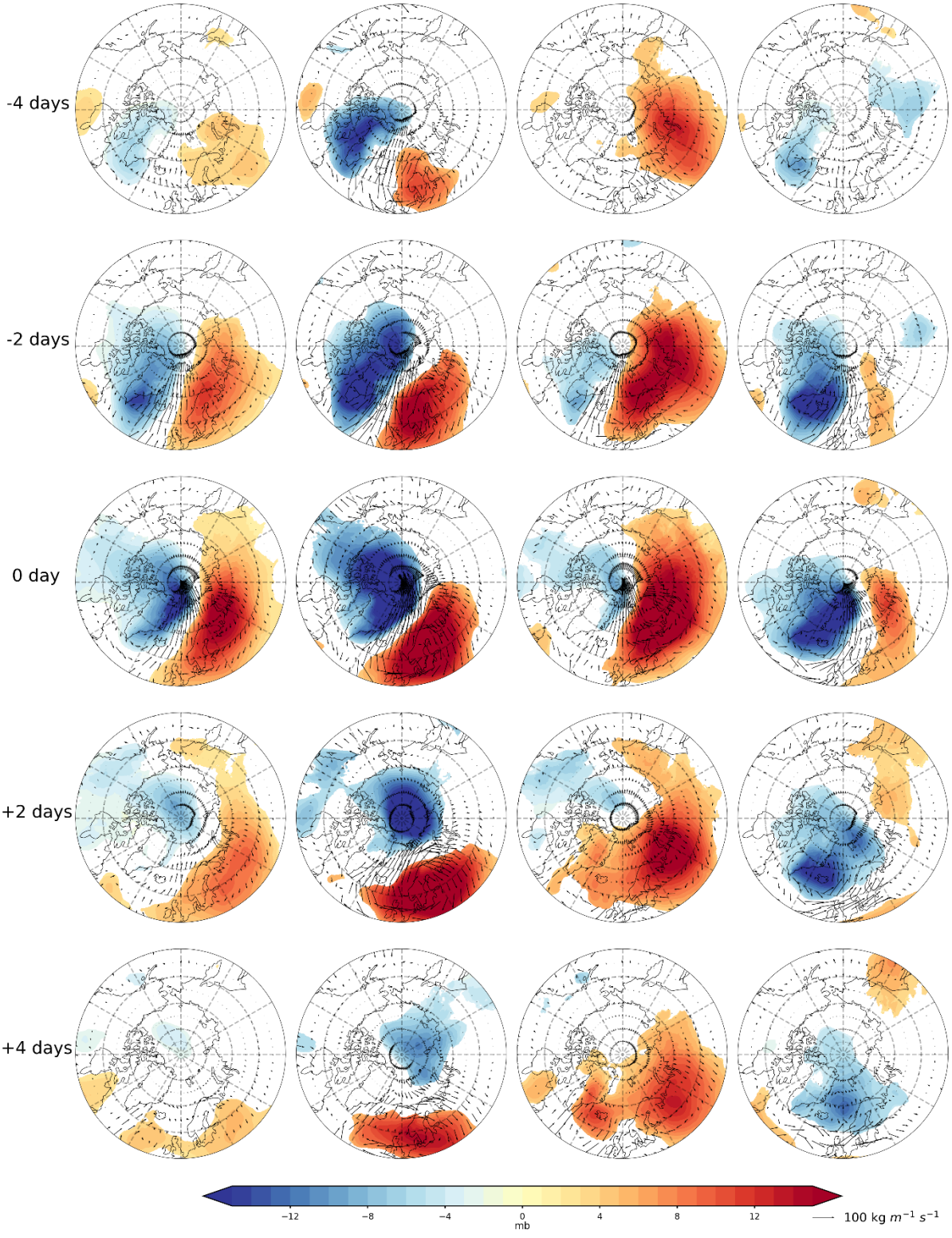

https://doi.org/10.5194/egusphere-2023-2018
Preprint. Discussion started: 20 September 2023

Figure 9. Temporal evolution of the large-scale circulation associated with the concurrent warming events. The shaded contours show the SLP anomalies, and the vectors represent the IVT anomalies. The 1st column describes the composites for all the concurrent warming events. The 2nd, 3rd, and 4th columns show the composites for the 1st, 2nd, and 3rd cluster, respectively, obtained from K-means clustering. Only anomalies that are significant at the 0.05 level based on the Student's t-test are shown. See the definition of concurrent warming events in the text. Day 0 indicates the time with the largest area where temperature exceeds 0℃.

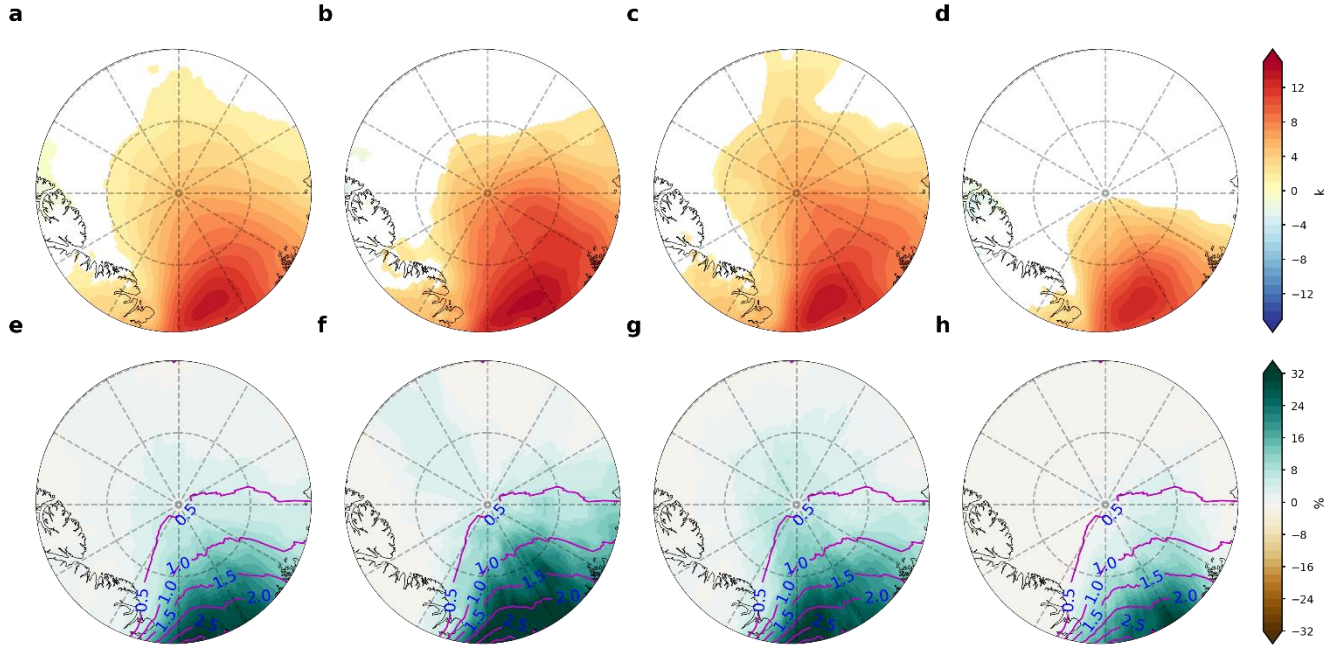

Figure 10. Same as Fig. 9, but for the T2m anomalies and AR frequency during the peak of the concurrent warming events. The peak of the concurrent warming events is defined as the time when the areas with temperature above 0℃ reach maximum. The purple line contours in (e) – (h) represent the climatology of winter AR frequency.

https://doi.org/10.5194/egusphere-2023-2018
Preprint. Discussion started: 20 September 2023

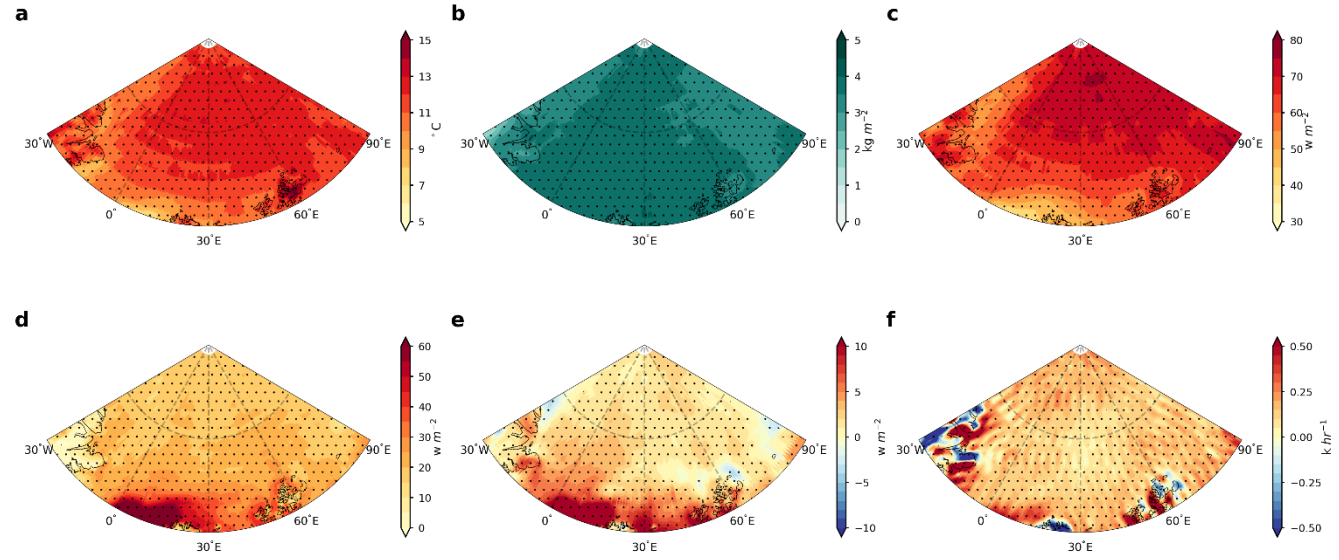

Figure 11. Spatial distribution of the anomalies of (a) T2m, (b) IWV, (c) DLW, (d) SHF, (e) LHF and temperature advection during AR days. Stippled areas indicate anomalies are significant at the 0.05 level based on the Student's t-test.

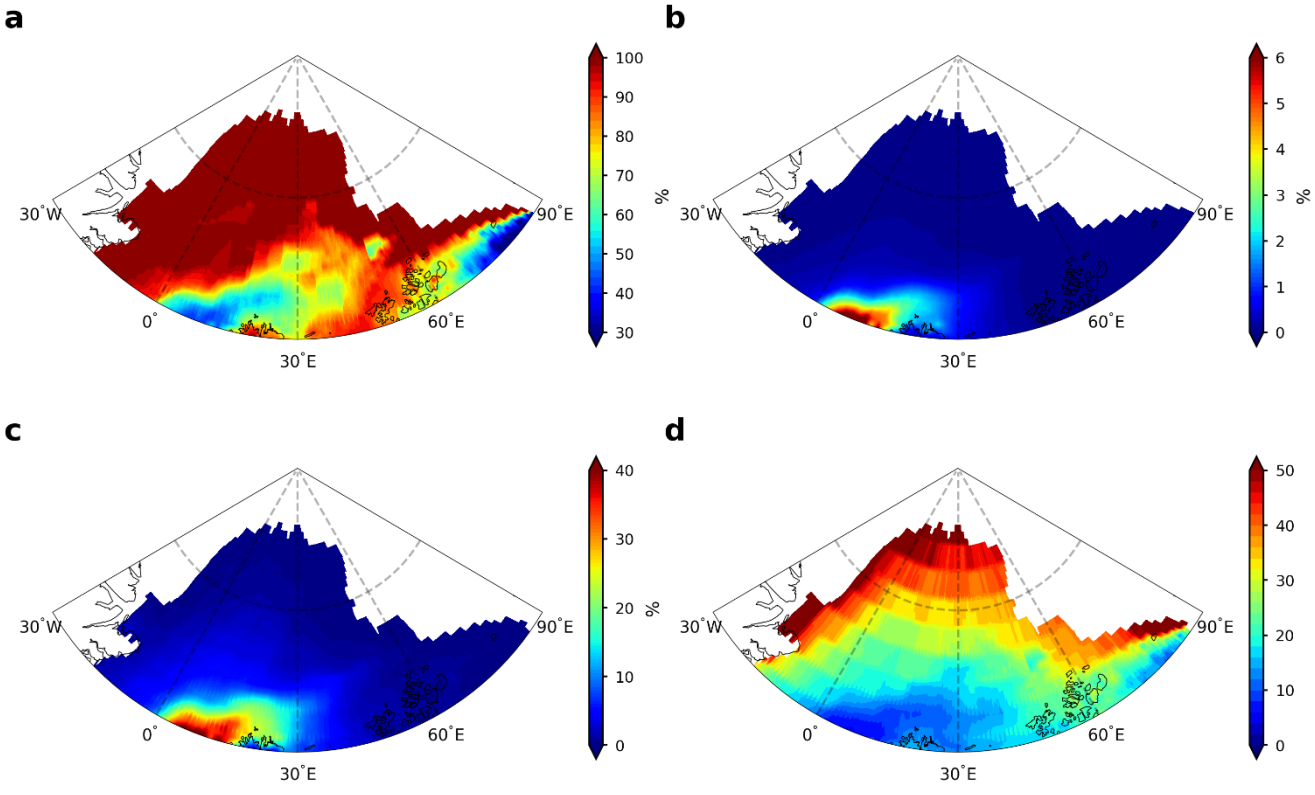

660

https://doi.org/10.5194/egusphere-2023-2018
Preprint. Discussion started: 20 September 2023

Figure 12. Spatial distribution of (a) the fraction of warming events that occurs during AR days, (b) the fraction of time for all winter hourly snapshots from 1979-2021 with T2m above 0℃, (c) the fraction of time for all AR day hourly snapshots from 1979-2021 with T2m above 0℃, and (d) the risk ratio, which is calculated by dividing (c) by (b).

665

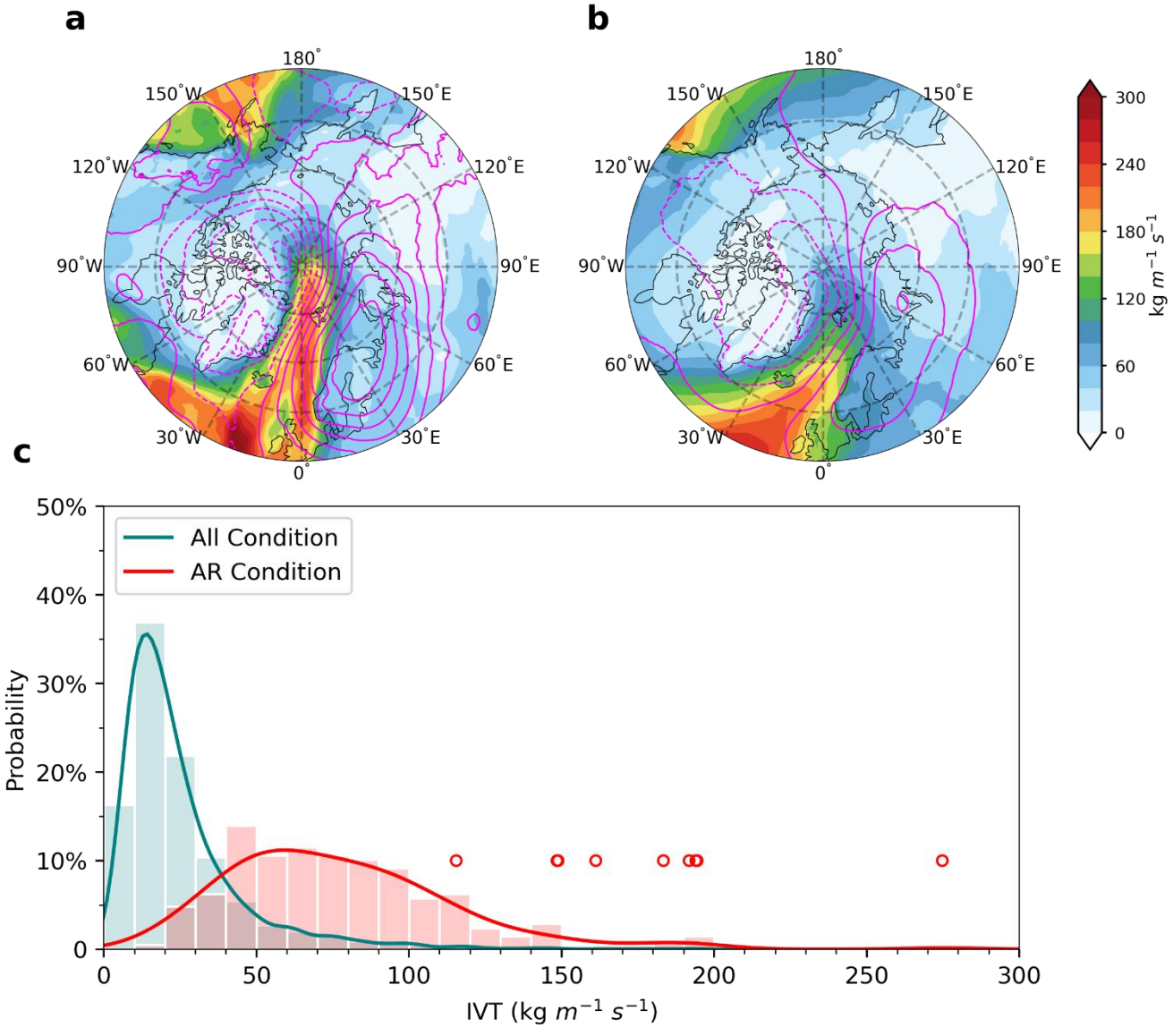

Figure 13. Composites of IVT (shaded contours) and SLP anomalies (line contours, solid lines denote positive values while dashed lines denote negative values) for (a) the nine days with warming events occurring poleward of 85°N, (b) all the days with ARs intercepting 85°N between 15°W-60°E, but no warming events found poleward of 85°N. (c) Probability density function of the daily IVT averaged over regions

https://doi.org/10.5194/egusphere-2023-2018
Preprint. Discussion started: 20 September 2023

poleward of 85˚N and between 15˚W-60˚E. The green bars/line are for all the winter days from 1979-2021, red bars/line are for the days with ARs intercepting 85˚N between 15˚W-60˚E. The open circles are for the nine days with warming events occurring poleward of 85˚N.

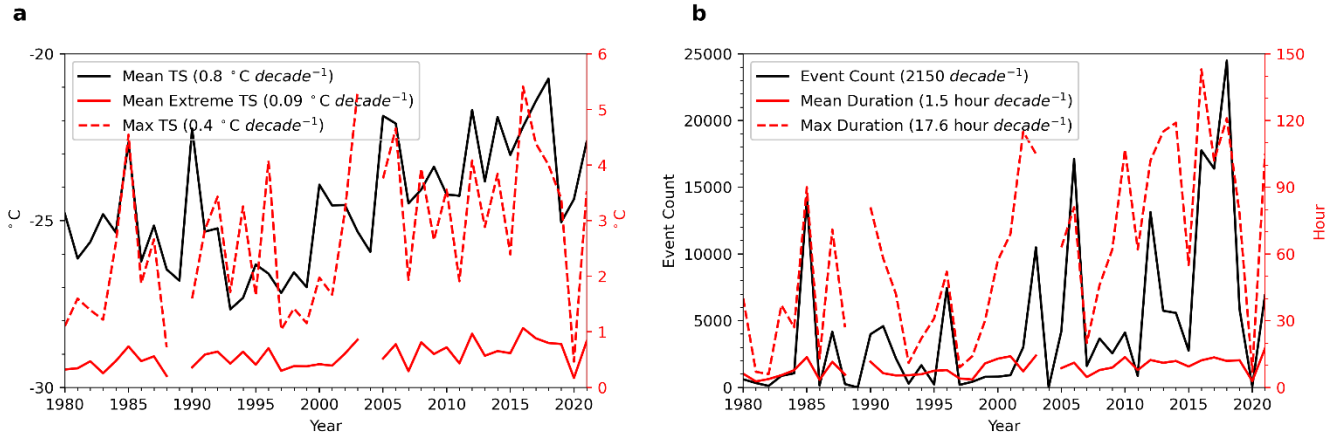

Figure 14. Trends in (a) the area-weighted spatial mean T2m (black solid line), mean T2m only for those above 0℃ (red solid line) and the seasonal maximum hourly T2m (red dashed line) over the high Arctic. (b) is the same as (a), but for the trends in event count (black solid line), mean event duration (red solid line) and seasonal maximum event duration (red dashed line). All trends are significant at the 0.05 level based on the Student's t-test.